Cardiovascular Diabetology

RESEARCH

Open Access

Elevated glucose levels increase vascular calcification risk by disrupting extracellular pyrophosphate metabolism

Alicia Flores-Roco[1,2], Belinda M. Lago[1,2] and Ricardo Villa-Bellosta[1,2,3,4*]

Abstract

Background Vascular calcification is a major contributor to cardiovascular disease, especially diabetes, where it exacerbates morbidity and mortality. Although pyrophosphate is a recognized natural inhibitor of vascular calcification, there have been no prior studies examining its specific deficiency in diabetic conditions. This study is the first to analyze the direct link between elevated glucose levels and disruptions in extracellular pyrophosphate metabolism.

Methods Rat aortic smooth muscle cells, streptozotocin (STZ)-induced diabetic rats, and diabetic human aortic smooth muscle cells were used to assess the effects of elevated glucose levels on pyrophosphate metabolism and vascular calcification. The techniques used include extracellular pyrophosphate metabolism assays, thin-layer chromatography, phosphate-induced calcification assays, BrdU incorporation for DNA synthesis, aortic smooth muscle cell viability and proliferation assays, and quantitative PCR for enzyme expression analysis. Additionally, extracellular pyrophosphate metabolism was examined through the use of radiolabeled isotopes to track ATP and pyrophosphate transformations.

Results Elevated glucose led to a significant reduction in extracellular pyrophosphate across all diabetic models. This metabolic disruption was marked by notable downregulation of both the expression and activity of ectonucleotide pyrophosphatase/phosphodiesterase 1, a key enzyme that converts ATP to pyrophosphate. We also observed an upregulation of ectonucleoside triphosphate diphosphohydrolase 1, which preferentially hydrolyzes ATP to inorganic phosphate rather than pyrophosphate. Moreover, tissue-nonspecific alkaline phosphatase activity was markedly elevated across all diabetic models. This shift in enzyme activity significantly reduced the pyrophosphate/phosphate ratio. In addition, we noted a marked downregulation of matrix Gla protein, another inhibitor of vascular calcification. The impaired pyrophosphate metabolism was further corroborated by calcification experiments across all three diabetic models, which demonstrated an increased propensity for vascular calcification.

Conclusions This study demonstrated that diabetes-induced high glucose disrupts extracellular pyrophosphate metabolism, compromising its protective role against vascular calcification. These findings identify pyrophosphate deficiency as a potential mechanism in diabetic vascular calcification, highlighting a new therapeutic target.

*Correspondence:
Ricardo Villa-Bellosta
ricardo.villa@usc.es

Full list of author information is available at the end of the article

Strategies aimed at restoring or enhancing pyrophosphate levels may offer significant potential in mitigating cardiovascular complications in diabetic patients, meriting further investigation.

Graphical abstract

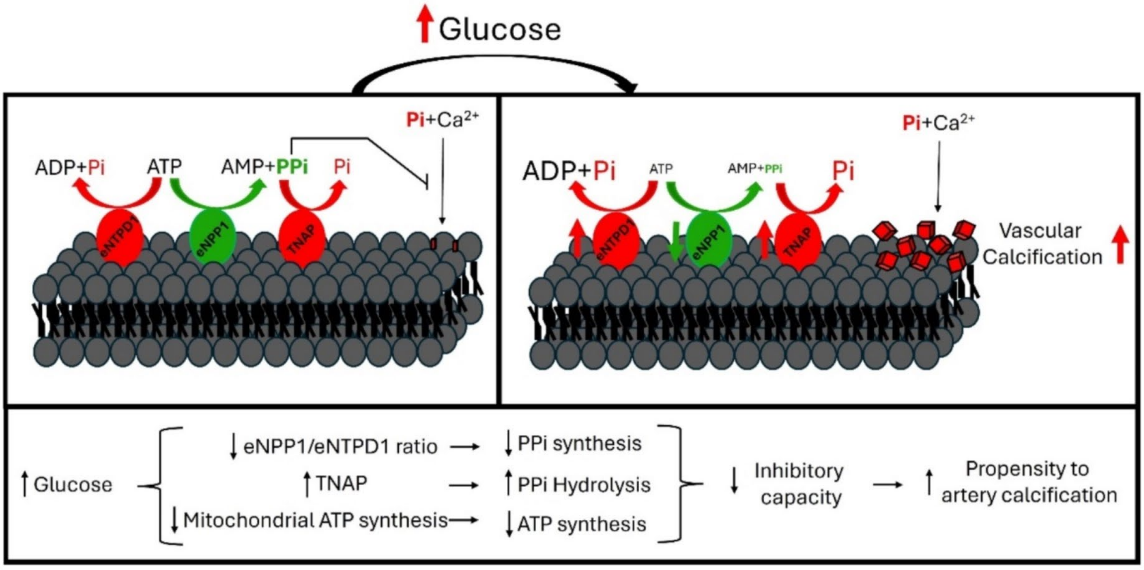

Keywords Vascular calcification, Diabetes, Pyrophosphate, ATP, Aging, Phosphate

Background

Diabetes is a chronic metabolic disorder characterized by elevated blood glucose levels. There are two primary types of diabetes [1, 2]. Type 1 diabetes occurs when the body's immune system mistakenly attacks and destroys insulin-producing beta cells in the pancreas. This leads to little or no insulin production, resulting in high blood sugar levels. Type 1 diabetes is typically diagnosed in children and young adults, although it can develop at any age. Individuals with type 1 diabetes require lifelong insulin therapy to manage their condition. Type 2 diabetes usually develops in adulthood but is increasingly being diagnosed in children and adolescents. In type 2 diabetes, the body becomes resistant to the effects of insulin, or the pancreas fails to produce enough insulin to maintain normal blood glucose levels, leading to chronically elevated blood sugar.

Both types of diabetes can lead to serious complications if not properly managed, including cardiovascular disease, kidney disease (nephropathy), nerve damage (neuropathy), and eye damage (retinopathy) [3, 4]. Diabetes significantly increases the risk of cardiovascular events such as heart attack, stroke, and peripheral artery disease [5]. A particularly concerning complication is vascular calcification, a pathological process characterized by the deposition of calcium phosphate crystals, primarily hydroxyapatite, within the walls of blood vessels. This condition most commonly affects arteries, including those supplying the heart (coronary arteries), brain (cerebral arteries), and peripheral tissues (peripheral arteries) [4].

Vascular calcification is a major contributor to cardiovascular morbidity and mortality in individuals with diabetes [6, 7]. It is closely associated with several key mechanisms identified in previous studies, including hyperglycemia, which promotes advanced glycation end-product (AGE) formation and oxidative stress; endothelial dysfunction, which impairs vasodilation and promotes vascular stiffness; dyslipidemia, characterized by high levels of LDL cholesterol that increase lipid deposition and inflammatory cell recruitment in vessel walls; chronic inflammation, which triggers the release

of proinflammatory cytokines and promotes vascular smooth muscle cell osteogenic differentiation; and mineral imbalance, involving dysregulated calcium and phosphate homeostasis that accelerates calcification processes in vascular tissues [8–10]. However, despite this understanding, to our knowledge, no studies have examined the role of extracellular pyrophosphate, a known inhibitor of calcification, in the development of vascular calcification under diabetic conditions.

Extracellular pyrophosphate metabolism involves biochemical processes that regulate and utilize pyrophosphate molecules outside of cells [11, 12]. Pyrophosphate is a crucial molecule with roles in various physiological functions, including bone mineralization, energy metabolism, and the regulation of vascular calcification. In the context of diabetes and vascular calcification, abnormalities in extracellular pyrophosphate metabolism can have significant consequences [13]. Disruption of normal pyrophosphate metabolism may result in reduced levels of pyrophosphate [14], a natural inhibitor of hydroxyapatite crystal formation and vascular calcification [13]. This imbalance can contribute to the development of vascular calcification, a common complication of diabetes that significantly increases cardiovascular risk [15].

Studies have also shown that pyrophosphate not only acts as a physical inhibitor of mineral crystal formation but also functions as a signaling molecule that can modulate the expression of genes involved in mineralization processes [16–18]. For example, pyrophosphate upregulates osteopontin (OPN) expression through the ERK1/2 and p38 MAPK signaling pathways, enhancing the role of OPN as a mineralization inhibitor [19]. Similarly, pyrophosphate influences the expression of matrix Gla protein (MGP), another potent inhibitor of vascular and soft tissue calcification, by regulating pathways that affect extracellular matrix mineralization. This dual function of pyrophosphate—as a direct crystal inhibitor and a regulator of gene expression related to calcification—provides a new perspective on how pyrophosphate homeostasis may be crucial for preventing pathological calcification.

Pyrophosphate is metabolized into phosphate by tissue-nonspecific alkaline phosphatase (TNAP) in extracellular fluids [20, 21]. Conversely, extracellular pyrophosphate is produced by ectonucleotide pyrophosphatase/phosphodiesterase (eNPP), which hydrolyzes extracellular adenosine-5′-triphosphate (ATP) to generate pyrophosphate and AMP (adenosine-5′-monophosphate) [22, 23]. In vascular smooth muscle cells and the aorta, the primary source of extracellular pyrophosphate is the hydrolysis of ATP by eNPP1 [24, 25]. Mutations in eNPP1 can lead to generalized arterial calcification in infancy, a condition marked by widespread arterial calcification in humans [26]. Additionally, the ectonucleoside triphosphate diphosphohydrolase (eNTPD) family, particularly eNTPD1, which is predominant in rat aortas [24], competes with eNPP for ATP substrate. eNTPD1 is responsible for approximately 90% of ATP hydrolysis in these tissues [24, 25]. While eNTPD1 is known primarily for its role in regulating purine receptor signaling, recent evidence suggests a direct association with vascular calcification [14, 27]. By hydrolyzing ATP to phosphate, eNTPD1 may reduce the availability of ATP for conversion to pyrophosphate by eNPP1, thereby potentially promoting calcification [14, 27]. Finally, ATP plays a critical role in preventing vascular calcification by serving as a source of pyrophosphate and directly inhibiting the formation of calcium phosphate crystals (CPCs) [27, 28].

Moreover, the progressive ankylosis (ANK) gene plays a role in regulating extracellular pyrophosphate levels and preventing pathological calcification [29]. Mutations in the ANK gene lead to a severe form of generalized joint calcification and arthritis, as observed in mouse models. Loss of ANK function in $ANK^{-/-}$ mice causes excessive hydroxyapatite formation, highlighting its role in controlling mineralization. Cells from ANK-deficient mice exhibit significantly reduced extracellular pyrophosphate levels, whereas the overexpression of ANK in cultured cells leads to increased extracellular pyrophosphate, highlighting ANK's essential function in maintaining pyrophosphate homeostasis and preventing pathological tissue calcification and arthritis [29].

The interplay of these pathophysiological mechanisms highlights the increased risk of vascular calcification in individuals with diabetes [5, 7]. Vascular calcification is a dynamic process driven by multiple factors, including the metabolic disturbances associated with diabetes [6, 30, 31]. Given its significant impact on cardiovascular health, vascular calcification is a critical therapeutic target in the management of diabetes. This underscores the need for comprehensive strategies to mitigate cardiovascular risk in affected individuals.

To our knowledge, there are currently no studies directly linking pyrophosphate deficiency with diabetes. Although pyrophosphate is recognized as a natural inhibitor of vascular calcification, its direct association with diabetes has not been established. This study specifically examines extracellular pyrophosphate metabolism in the context of hyperglycemia, aiming to identify novel risk factors and therapeutic targets to address this widespread disease.

Methods

Animals

Male Sprague–Dawley rats (8–9 weeks old) were obtained from Charles River Laboratories (France). To induce diabetes, a single intraperitoneal injection of streptozotocin (55 mg/kg body weight, Sigma–Aldrich) was administered in a 0.9% NaCl solution. The control rats received

an equivalent volume of isotonic saline solution. The protocol was approved by the ethics committee (PROEX 427/15) and conformed to directive 2010/63EU and recommendation 2007/526/EC on the protection of animals used for experimental and other scientific purposes, enforced in Spanish law under RD1201/2005.

ASMC isolation and culture

Rat aortic smooth muscle cells (ASMCs) were isolated using a double digestion protocol with collagenase [32]. The ASMCs were cultured in Minimum Essential Medium Eagle (MEM) supplemented with 2 mM L-glutamine, 100 IU/ml penicillin, 100 µg/ml streptomycin, and 10% fetal bovine serum at 37 °C in a humidified atmosphere containing 5% CO_2. All cell culture reagents were obtained from Invitrogen (Paisley, UK). The control group was maintained in MEM with a glucose concentration of 1 g/L (control medium). To prepare glucose-enriched medium, MEM supplemented with glucose (Sigma–Aldrich) was filtered through a 0.22 µm filter (PES033S0221, Scharlab, Barcelona, Spain), resulting in a final concentration of 4.5 g/L. After initial trypsinization (passage 1), the cells were incubated in either 1 g/L or 4.5 g/L glucose MEM and passaged to passage 12. The cells were maintained at a 1:3 split ratio during each trypsinization step. The medium was changed every 2–3 days.

Human diabetic and non-diabetic aortic smooth muscle cells (Lonza, Walkersville, USA) were cultured in SmGM-2 medium (Lonza) according to the manufacturer's instructions. The cells were incubated at 37 °C in a humidified atmosphere containing 5% CO_2. A 1:3 split ratio was used during each trypsinization step to maintain the cultures.

Cell proliferation

Cell counting was performed regularly over a 6-week period to assess the division rate of rat aortic smooth muscle cells cultured under both experimental conditions. A Neubauer counting chamber (717805, Brand™, Arnedo, Spain), also known as a hemocytometer, was used for accurate cell counting. Cell passages were carried out upon reaching 50% confluence, using trypsin (Thermo Fisher).

Cell proliferation was evaluated by measuring the incorporation of 5-bromodeoxyuridine (BrdU) via the BrdU Cell Proliferation ELISA Kit (Abcam, ab126556) following the manufacturer's protocol. The absorbance was read at dual wavelengths of 450/550 nm using a Varioskan™ LUX multimode microplate reader, and the results are expressed as the optical density (OD) per cell.

Cell viability

The viability of aortic smooth muscle cells was evaluated via the PrestoBlue™ Cell Viability Reagent (A13261; Invitrogen) according to the manufacturer's protocol. This assay utilizes resazurin as a redox indicator to measure cellular viability. Upon incubation with viable cells, resazurin, a cell-permeable, nonfluorescent blue dye, is reduced by mitochondrial oxidoreductase enzymes in metabolically active cells to resorufin, a pink, fluorescent compound.

Briefly, subconfluent aortic smooth muscle cells were dissociated using trypsin (200 U/ml, Thermo Fisher) and counted. Five serial dilutions of the cells were prepared in the appropriate culture medium for each experimental group. Following the manufacturer's instructions, 90 µL of the cell suspensions and 10 µL of PrestoBlue reagent were added to each well of a 96-well plate, resulting in a final volume of 100 µL per well. The plate was incubated in the dark at 37 °C, and the absorbance was measured at 570 nm (to detect resorufin) and 600 nm (background) at 30-minute intervals over a 2-hour period using a Varioskan™ LUX multimode microplate reader.

ATP and pyrophosphate quantification

The intracellular and extracellular ATP levels were measured using a coupled luciferin/luciferase reaction with an ATP Determination Kit (Invitrogen) following the manufacturer's instructions and previous studies [14, 27]. For intracellular ATP quantification, aortic smooth muscle cells were lysed in lysis buffer containing 50 mM Tris–HCl, 150 mM NaCl, and 0.1% Triton X-100 (pH 7.4). Intracellular ATP measurements were performed on cell lysates alongside ATP standards for calibration. Extracellular pyrophosphate was measured with an enzyme-linked bioluminescence assay as described previously [14]. ATP and pyrophosphate levels were normalized to the cellular protein content, which was quantified using the Pierce™ BCA Protein Assay Kit according to the manufacturer's instructions.

Mitochondrial ATP synthesis in digitonin-permeabilized aortic smooth muscle cells (2×10^6 cells) was evaluated via a kinetic luminescence assay based on the previous studies [14, 27].

Extracellular pyrophosphate metabolism

Aortic smooth muscle cells (ASMCs) or aortic rings were incubated in vitro or ex vivo, respectively, in Hank's balanced salt solution (HBSS, BE10-527 F, Lonza) containing specified concentrations of pyrophosphate (Sigma–Aldrich) and pyrophosphate-32 (Perkin-Elmer) or ATP (Sigma–Aldrich) and [γ-^{32}P]ATP (Perkin-Elmer). After the designated incubation periods, ATP and pyrophosphate were separated from orthophosphate as described in previous protocols [24, 27].

Briefly, 20 µL of the sample was mixed with 400 µL of ammonium molybdate (Sigma–Aldrich) to bind orthophosphate, followed by the addition of 0.75 mol/L sulfuric acid (Sigma–Aldrich). The solution was then extracted with 800 µL of an isobutanol/petroleum ether mixture (4:1; Sigma–Aldrich) to separate phosphomolybdate from pyrophosphate and ATP. A 400 µL aliquot of the organic phase containing phosphomolybdate was collected, and its radioactivity was measured.

The same aortic rings were used for both the ATP and pyrophosphate hydrolysis assays. Following the ATP hydrolysis assays, the rings were washed five times with HBSS before the pyrophosphate hydrolysis assays were conducted. Finally, the aortic rings were dried and weighed.

To analyze the products released during ATP hydrolysis, ASMCs or aortic rings were incubated in HBSS containing ATP and [γ-^{32}P]ATP at final concentrations of 1 µmol/L and 10 µCi/mL, respectively. After the designated incubation periods, the production of phosphate-32 (^{32}Pi) and pyrophosphate-32 (^{32}PPi) was determined by chromatography using PEI-cellulose plates (50488-25EA-F, Sigma–Aldrich). The plates were developed with 650 mmol/L K_2HPO_4 (Sigma–Aldrich) at pH 3.0, following previous studies. The resulting spots were excised and analyzed via liquid scintillation counting via UltraGold (6013329, Perkin-Elmer).

Recombinant enzymes and inhibitors

The recombinant enzymes eNPP1 (catalog number 6136-EN) and eNTPD1 (catalog number 4397-EN) were obtained from R&D Systems (Minneapolis, MN, USA). The eNTPD1 inhibitor PSB609 [33, 34] was obtained from Tocris Bioscience (Minneapolis, MN, USA; catalog number 2573). The TNAP inhibitor SBI425 [35, 36] was sourced from Sigma–Aldrich (catalog number SML2935).

Real-time polymerase chain reaction

Total RNA was isolated using TRIzol reagent (Invitrogen), and cDNA synthesis was performed with the Superscript III cDNA Synthesis System (Invitrogen) following the manufacturer's instructions. Relative quantification of the expression of the rat genes BMP2, SM22α, TNAP, eNTPD1, and eNPP1 was conducted via real-time PCR with SYBR Green according to the manufacturer's protocol. The sequences of primers used for amplification were as follows [25]: BMP2: 5′-GTTCTGTCCCTACTGATGAG-3′ (forward) and 5′-ATTCGGTGCTGGAAACTAC-3′ (reverse); SM22α: 5′-CAGACTGTTGACCTCTTTGAAG-3′ (forward) and 5′-TCTTATGCTCCTGGGCTTTC-3′ (reverse); TNAP: 5′-TGAATCGGAACAACCTGACTG-3′ (forward) and 5′-GCCTCCTTCCACTAGCAAGAA-3′ (reverse); eNTPD1: 5′-CAGGTTTCAAGTGGTGGGATT-3′ (forward) and 5′-GAAGGCACACTGGGAGTAAGG-3′ (reverse); eNPP1: 5′-AAGGTATGCCCAAGAAAGGAA-3′ (forward) and 5′-TTCTTGACTGCGGATGACTCT-3′ (reverse).

The comparative ΔΔCT method was used for quantification, with acidic ribosomal phosphoprotein (ARP) RNA serving as the endogenous reference. The primers used for rat ARP amplification were 5′-CACCTTCCCACTGGCTGAA-3′ (forward) and 5′-CACCTTCCCACTGGCTGAA-3′ (reverse).

ASMC calcification assay

Rat aortic smooth muscle cells (ASMCs) were cultured to confluence and subjected to a quiescence step by incubation overnight in culture medium containing 0.1% fetal bovine serum. Calcification assays were then performed by incubating the cells for 7 days in minimum essential medium (MEM) supplemented with 2 mM L-glutamine, 100 IU/ml penicillin, 100 µg/ml streptomycin, 0.1% fetal bovine serum, and 2 mmol/L phosphate (phosphate-calcifying medium), as previously described [32, 37]. The phosphate-calcifying medium and control medium were replaced daily. To quantify the calcium content in rat ASMCs, the wells were treated with 0.6 M HCl overnight at 4 °C, and the calcium levels were analyzed via a QuantiChrom Calcium Assay Kit (BioAssay Systems, Hayward, CA) via a colorimetric method. Cell fixation was carried out according to previous studies [37, 38].

Human aortic smooth muscle cells (ASMCs) were cultured to confluence in SmGM-2 medium and subjected to a quiescence step by incubating overnight in MEM containing 0.1% fetal bovine serum. Calcification assays were performed by incubating the cells for 4 days in minimum essential medium (MEM) supplemented with 2 mM L-glutamine, 100 IU/ml penicillin, 100 µg/ml streptomycin, 0.1% fetal bovine serum, and 10 µCi/mL calcium-45 as a radiotracer.

To quantify the calcium content in ASMCs, the wells were washed five times with 9 g/L NaCl, treated with 200 µL of 0.6 M HCl and incubated overnight at 4 °C to release calcium. Following incubation, 50 µL of the calcium-containing HCl solution was transferred to a liquid scintillation fluid (UltimaGold™, 6013329; Perkin Elmer), and radioactivity was measured via a Tri-Carb 2810TR liquid scintillation analyzer (Perkin Elmer).

Aorta isolation and calcification assay

The rats were euthanized via carbon dioxide inhalation, and the thoracic aorta tissue was perfused with saline and removed following previously published protocols [25, 32]. For calcification assays, aortic rings were cultured ex vivo at 37 °C with 5% CO_2 in minimum essential medium (MEM) supplemented with calcium-45 (^{45}Ca) as a radiotracer (Perkin Elmer, Boston), 2 mmol/L L-glutamine, 100 IU/mL penicillin, 100 µg/mL streptomycin,

and 0.1% fetal bovine serum. Aortic rings were further cultured in MEM supplemented with 2 mmol/L phosphate (KH_2PO_4/K_2HPO_4, pH 7.4) for calcification assays, whereas the control groups received 1 mmol/L phosphate. After 7 days of incubation, the aortic rings were dried, and the radioactivity was measured using liquid scintillation counting (Perkin Elmer Tri-Carb 2810TR).

Aortic staining

Rat aortas were embedded in optimal cutting temperature compound (Sakura, Alphen aan den Rijn, The Netherlands), and 5-µm cross-sections were prepared using a cryostat (Leica CM1940). The calcification of the aortic tissue was assessed through Alizarin Red and Von Kossa staining, while the cell content and tissue architecture were visualized via hematoxylin and eosin (H&E) staining.

Analytical parameters

For the analytical parameters shown in Fig. 1, blood samples were collected from euthanized rats into serum or heparinized tubes and centrifuged to separate the serum or plasma, respectively. Liver glycogen, as well as plasma glucose, insulin, AGEs, GSP, and TNFα, were quantified using the following kits according to the manufacturer's protocols: a glycogen assay kit (Abcam, ab65620), a glucose assay kit (Abcam, ab65333), a rat insulin ELISA kit (Thermo Fisher Scientific), a rat advanced glycation end products (AGEs) ELISA kit (RTEB0188), a glycated serum protein ELISA kit (ABIN771898), and a rat TNFα ELISA kit (Thermo Fisher Scientific).

Immunoblotting and ELISA

Immunoblot assays were conducted via a chemiluminescent detection method with a Millipore kit, as previously described [14]. Primary antibodies against TNAP (LS-C171640), eNPP1 (LS-C780091), and eNTPD1 (LS-C387669) were obtained from LSBio (Shirley, MA, USA) and used following the manufacturer's protocols. For the sandwich ELISAs, commercial kits for eNPP1 (LS-F33284), eNTPD1 (LS-F20306), TNAP (LS-F4993), MGP (LS-F6344), OPN (LS-F2199), BMP2 (LS-F2407), SM22α (LS-F7231), and Cbfa1/Runx2 (LS-F53973) were also purchased from LSBio and used according to the manufacturer's instructions.

Statistical analysis

The Kolmogorov–Smirnov test was used to assess the normality of the data. Student's *t* test or one-way ANOVA and Tukey's multiple comparison post hoc test were used for statistical analyses (according to the figure legends). Statistical significance was determined via GraphPad Prism 5 software.

Results

Elevated glucose levels reduce the viability of aortic smooth muscle cells

Given that cell viability and proliferation are closely linked to the cellular energy profile, they may significantly

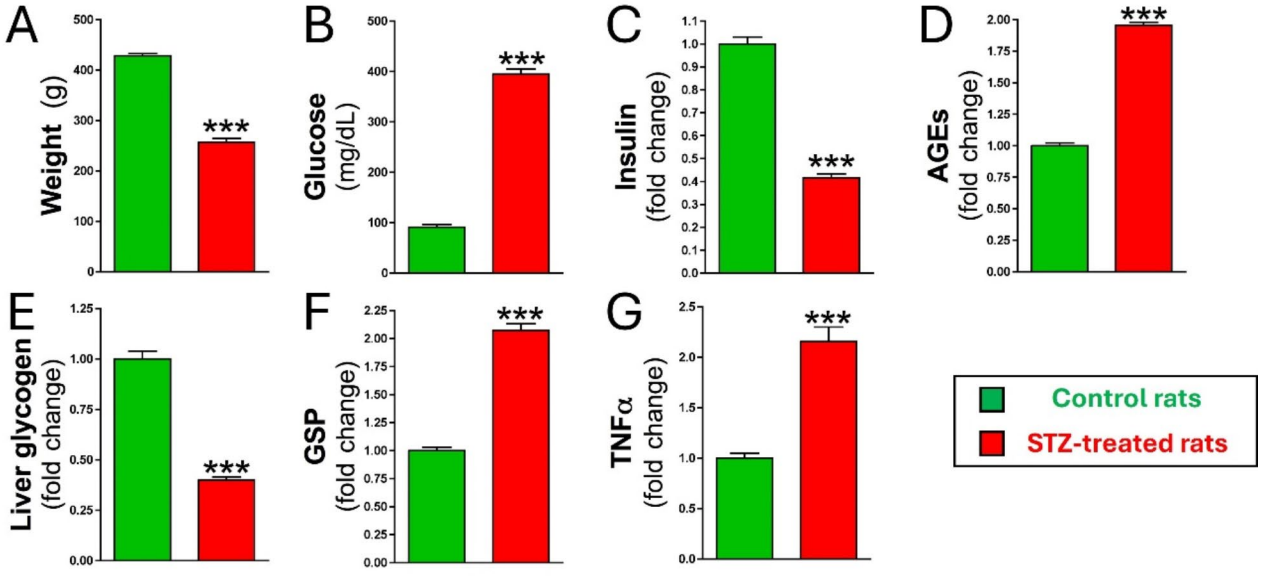

Fig. 1 Impairment of glucose homeostasis in STZ-treated rats.**A** Body weight, **B** blood glucose levels, **C** blood insulin levels, **D** advanced glycation end products (AGEs), **E** liver glycogen content, **F** glycated serum protein (GSP), and **G** tumor necrosis factor-alpha (TNFα) levels in plasma from STZ-treated (left, green) and control rats (right, red). The data are shown as the mean ± SEM ($n = 12$). Statistical significance was assessed via Student's t test. Asterisks denote significant differences, with ***$P < 0.001$

impact ATP synthesis and, consequently, play a critical role in maintaining extracellular pyrophosphate homeostasis. Therefore, we initially conducted a comparative assessment of the proliferative capacity of primary aortic smooth muscle cells (ASMCs) subjected to varying glucose concentrations. These cells were exposed to glucose concentrations of either 1 g/L or 4.5 g/L over the course of several weeks (Fig. 2).

Daily monitoring of cell growth under an optical microscope was essential because of the varying intervals between cell passages across the experimental groups, with 50% confluence not consistently achieved within the same timeframe. After 15 days, differences in growth between the two groups were clearly observable under the microscope.

Microscopic examination revealed strikingly similar cellular morphologies across both experimental groups (Fig. 2A). However, compared with control ASMCs (1 g/L), ASMCs cultured in high-glucose medium (4.5 g/L) exhibited significantly reduced proliferation. Notably, their daily division rate was ~ 54% lower than that of the control cells, with a rate of 0.15±0.03 divisions per day compared with 0.33±0.02 divisions per day in the controls (Fig. 2B and C).

To assess DNA replication status, we evaluated the incorporation of 5-bromodeoxyuridine (BrdU) in ASMCs (Fig. 2D). Compared with control cells, cells exposed to high-glucose medium showed a 66% slower rate of DNA synthesis (1±0.07 vs. 0.35±0.01). Additionally, cellular viability, as measured by mitochondrial dehydrogenase activity, was significantly reduced to 55.36±5.3% in ASMCs cultured in high-glucose medium compared to controls (Fig. 2E). Moreover, mitochondrial ATP synthesis was significantly lower (59.44±2.78%) in ASMCs exposed to high glucose than in control ASMCs (Fig. 2F). Finally, compared with those in control cells, both the intracellular and the extracellular ATP concentrations in ASMCs exposed to high-glucose medium decreased significantly to 28.21±3.93% and 31.09±1.29%, respectively (Fig. 2G and H).

High glucose levels impair pyrophosphate synthesis in aortic smooth muscle cells

Aortic smooth muscle cells exposed to elevated glucose concentrations exhibited a significant reduction in extracellular pyrophosphate levels, decreasing to 15.0±1.71% compared to cells maintained under control glucose conditions (Fig. 3A). Unexpectedly, high-glucose conditions also resulted in a pronounced decrease in the extracellular pyrophosphate-to-ATP (PPi/ATP) ratio, which decreased to 47.64±5.96% after one month (Fig. 3B), suggesting marked impairment of extracellular pyrophosphate metabolism.

To assess extracellular pyrophosphate metabolism, three analytical approaches were utilized. First, mRNA expression analysis of key enzymes involved in extracellular pyrophosphate metabolism revealed substantial upregulation of eNTPD1 (catalyzing ATP to phosphate)

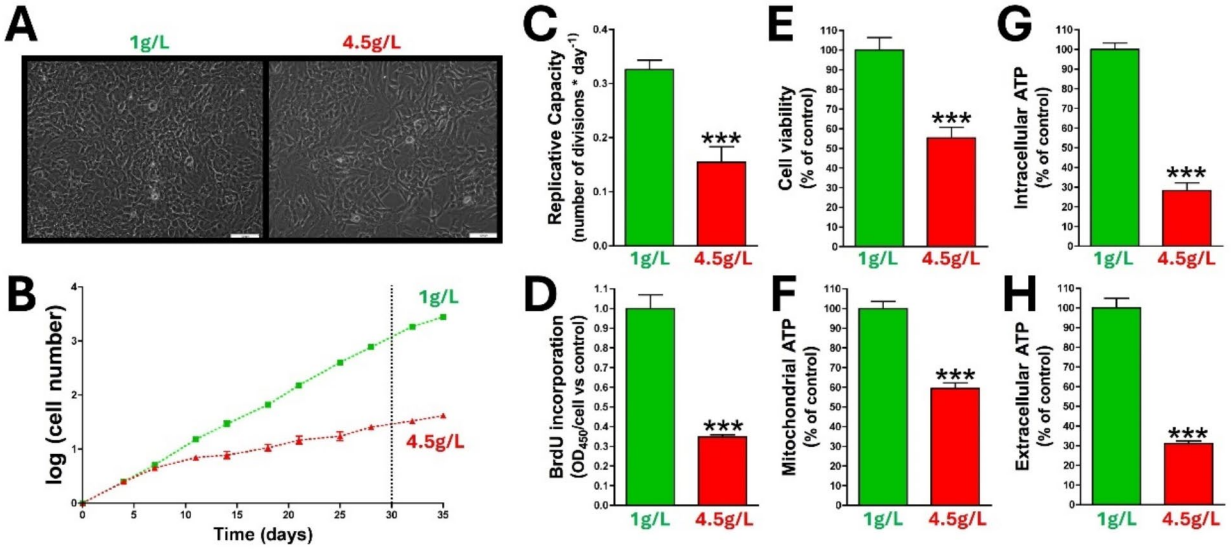

Fig. 2 High glucose levels impair ASMC viability. Aortic smooth muscle cells (ASMCs) were incubated in MEM containing either 1 g/L (green) or 4.5 g/L (red) glucose. **A** Representative microscopy images (10x; scale bar: 100 µm) of ASMCs after 30 days of incubation. **B** Number of replicative cells at the indicated time points, with cell counting starting at passage 2 and continuing until day 35. **C** Mean number of cell divisions per day over the first 30 days ($n=10$). **D** Incorporation of 5-bromodeoxyuridine (BrdU) into DNA as a measure of replication ($n=10$). **E** Cell viability ($n=16$). **F** Mitochondrial ATP synthesis ($n=16$). **G** Intracellular ATP content ($n=12$). **H** Extracellular ATP content ($n=16$). The data are shown as the mean ± SEM. Statistical analysis was performed via Student's t test, with asterisks indicating a significant difference at ***$P<0.001$

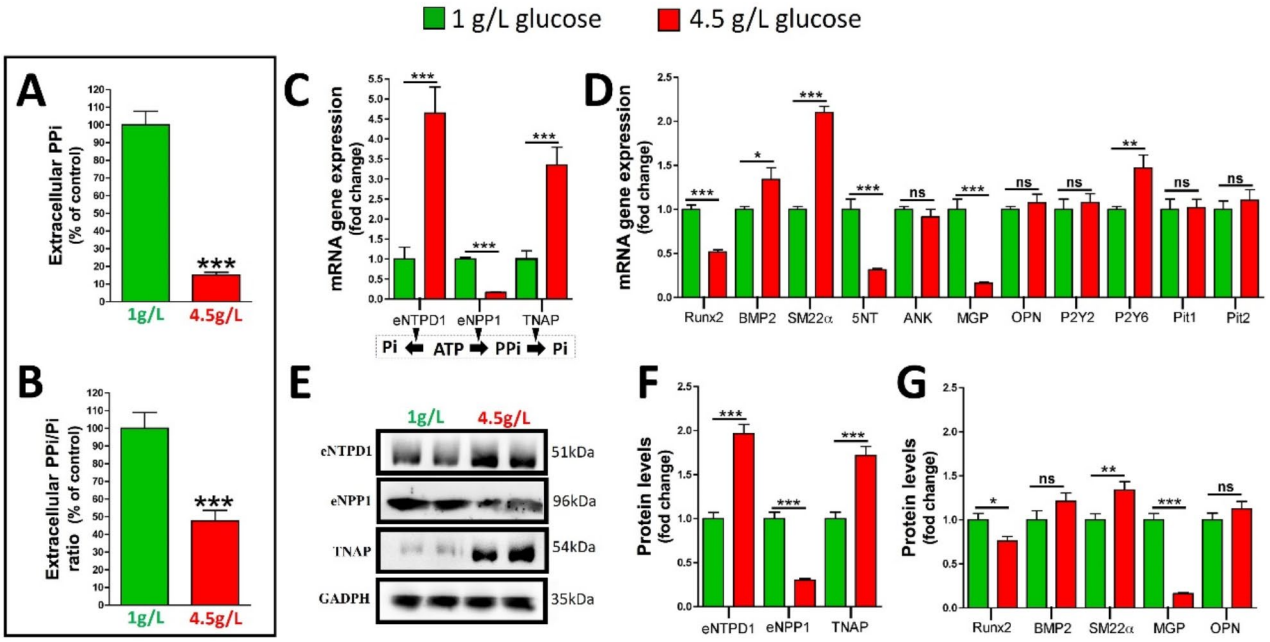

Fig. 3 Impact of high glucose on extracellular pyrophosphate metabolism. Aortic smooth muscle cells were cultured for one month in media containing either low (1 g/L) or high (4.5 g/L) glucose. **A** Measurement of extracellular pyrophosphate levels. **B** Extracellular pyrophosphate-to-ATP ratio. **C**, **D** Analysis of the gene expression of key enzymes involved in extracellular pyrophosphate metabolism, including eNTPD1, eNPP1, and TNAP, from isolated total RNA. **(E)** Immunoblot analysis of proteins associated with extracellular pyrophosphate metabolism. **F**, **G** Quantification of protein levels via ELISA, highlighting significant differences. The data are shown as the mean ± SEM, with data derived from 4 independent experiments, each containing 4 replicate plates. Statistical significance was determined via Student's *t* test, with asterisks denoting significance levels: *$P < 0.05$; **$P < 0.01$; ***$P < 0.001$

and TNAP (catalyzing pyrophosphate to phosphate), with mRNA levels increasing by 4.7-fold and 3.3-fold, respectively, in ASMCs exposed to 4.5 g/L glucose compared with the 1 g/L glucose control (Fig. 3C). In contrast, eNPP1 (catalyzing ATP to pyrophosphate conversion) mRNA expression was significantly downregulated, showing a 6.1-fold decrease in high-glucose conditions relative to the control. Figure 3D shows the mRNA expression profiles of additional genes, including the osteogenic markers BMP2 and SM22α, which were significantly overexpressed under the 4.5 g/L glucose condition compared with the control conditions. Both the Runx2 and matrix Gla proteins, which are well-established inhibitors of vascular calcification, exhibited notable reductions in mRNA expression under high-glucose conditions relative to the control. Additionally, ecto-5'-nucleotidase (5NT, which catalyzes AMP to phosphate and adenosine) and P2Y purinoceptor 6 were significantly downregulated and upregulated, respectively, under 4.5 g/L glucose conditions compared with the control.

Second, protein expression was analyzed. Figure 3E shows immunoblots of the three main enzymes involved in extracellular pyrophosphate metabolism, while Fig. 3F shows quantified protein levels via ELISA. In both analyses, there was a significant increase in eNTPD1 and TNAP protein levels under high-glucose conditions compared with those in the control. In contrast, eNPP1 protein levels were significantly lower under high-glucose conditions than under the control conditions. Additionally, the protein levels of the osteogenic marker SM22α significantly increased in high-glucose medium (Fig. 3G), whereas the protein levels of matrix Gla and Runx2 significantly decreased in high-glucose medium compared with those in the control.

Third, we aimed to evaluate the activity of the three primary enzymes involved in extracellular pyrophosphate metabolism by analyzing the products released during ATP hydrolysis. For this purpose, we employed thin-layer chromatography as outlined in previous studies (Fig. 4A) [24, 25, 27]. As shown in Fig. 4B, ATP hydrolysis was complete after one hour of incubation in ASMCs, according to our previous studies [25]. The addition of a specific TNAP inhibitor (SBI425) had no effect on pyrophosphate production from ATP hydrolysis, suggesting that the liberated pyrophosphate was not hydrolyzed by TNAP during the assay. In contrast, the addition of inorganic pyrophosphatase completely abolished pyrophosphate production (Fig. 4C). Notably, the pyrophosphate-to-phosphate ratio (Fig. 4D) resulting from ATP hydrolysis was significantly lower (6.1-fold) in ASMCs incubated with a high glucose concentration (0.12 ± 0.01) than in those incubated with a control glucose concentration (0.75 ± 0.07).

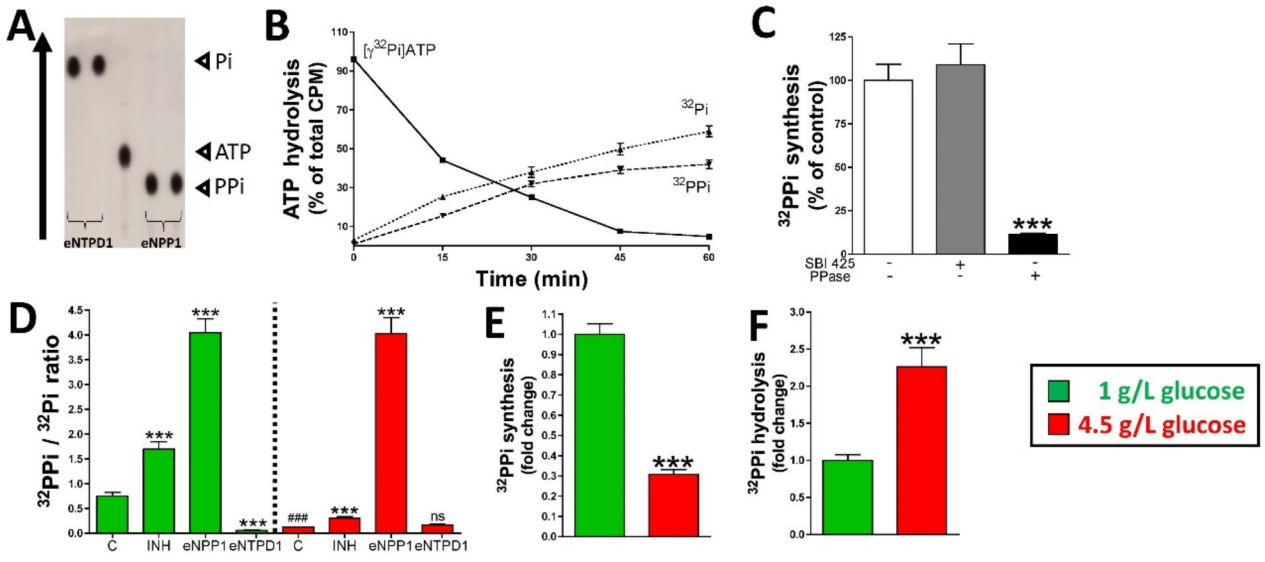

Fig. 4 High glucose levels impair the pyrophosphate-to-phosphate ratio. Aortic smooth muscle cells were incubated for one month in medium containing 1 g/L or 4.5 g/L glucose. **A** Autoradiograph displaying representative products from the hydrolysis of ATP (1 µmol/L ATP, 10 µCi/mL [γ^{32}Pi]ATP) incubated with or without recombinant eNPP1 (ectonucleotide pyrophosphatase/phosphodiesterase 1) or eNTPD1 (ectonucleoside triphosphate diphosphohydrolase 1) enzymes. Enzymatic hydrolysis generated radiolabeled ^{32}PPi (32-pyrophosphate) and ^{32}Pi (32-phosphate), which, alongside unreacted [γ^{32}Pi]ATP, were separated by thin-layer chromatography (TLC), as detailed in the Methods section. **B** Representative time course of ATP hydrolysis showing the products released over time. **C** Synthesis of the pyrophosphate ^{32}PPi via hydrolysis of [γ^{32}Pi]ATP (10 µCi/mL; 1 µmol/L ATP) in the absence or presence of 100 µmol/L SBI245 (a specific TNAP inhibitor) or inorganic pyrophosphatase (PPase). **D** The pyrophosphate-to-phosphate (^{32}PPi/^{32}Pi) ratio was quantified following hydrolysis of [γ^{32}Pi]ATP (10 µCi/mL; 1 µmol/L ATP) under various conditions: in the absence of inhibitors (Control), in the presence of an ectonucleoside triphosphate diphosphohydrolase (eNTPD) inhibitor (INH, 200 µmol/L), or with the recombinant enzymes eNPP1 and eNTPD1 (100 ng/mL). Experiments were conducted in media containing either physiological (1 g/L) or elevated (4.5 g/L) glucose concentrations. D) Synthesis of ^{32}PPi by hydrolysis of [γ^{32}Pi]ATP (10 µCi/mL and 1 µmol/L ATP). **E** Hydrolysis of ^{32}PPi (10 µCi/mL and 5 µmol/L PPi). The results are shown as the mean ± SEM (4 independent experiments with 4 plates per experiment). Student's t test (**E, F**) or one-way ANOVA with Tukey's post hoc test (**C, D**) was used for statistical analysis. Asterisks indicate a statistically significant difference compared with the control group: *$P < 0.05$; ***$P < 0.001$. ### Indicates a value of $P < 0.001$ compared with the control group (1 g/L)

Interestingly, the addition of an inhibitor of eNTPD activity (ATP-to-phosphate conversion) increased the pyrophosphate/phosphate ratio from ATP hydrolysis in ASMCs under both study conditions (1 g/L and 4.5 g/L glucose). However, this increase was significantly lower in the presence of 4.5 g/L glucose than in the presence of 1 g/L glucose (Fig. 4D). Furthermore, the addition of recombinant eNPP1 significantly elevated the pyrophosphate/phosphate ratio under both experimental conditions. In contrast, the addition of recombinant eNTPD1 significantly reduced the pyrophosphate/phosphate ratio in ASMCs incubated under control conditions (1 g/L glucose) but did not significantly differ under 4.5 g/L glucose. Together, these findings support our results indicating an increase in eNTPD activity and a reduction in eNPP activity in ASMCs incubated with 4.5 g/L glucose.

Moreover, the synthesis of pyrophosphate from ATP hydrolysis significantly decreased to 30.83±2.33% in ASMCs incubated in media supplemented with 4.5 g/L glucose over one month compared with the control group maintained in media supplemented with 1 g/L glucose (Fig. 4E). Additionally, pyrophosphate hydrolysis was markedly greater (to 226.1±25.76%) in cells exposed to glucose-enriched medium (4.5 g/L) than in control cells (Fig. 4F).

High glucose levels enhance phosphate-induced aortic smooth muscle cell calcification

Previous studies have demonstrated that calcification can occur independently of cellular activity, as observed in both cultured devitalized aortas [25] and fixed smooth muscle cells [38]. To investigate the impact of high glucose exposure on aortic smooth muscle cell (ASMC) calcification, ASMCs were incubated in phosphate-calcifying medium (2 mmol/L phosphate) under two glucose conditions: 1 g/L and 4.5 g/L. The calcification induced by phosphate was then evaluated in both live and fixed cells over a 7-day period (Fig. 5A).

Aortic smooth muscle cells incubated in a high-phosphate environment (Fig. 5B) presented a 5.5-fold increase in calcium deposition in live cells (25.42±1.46 µg/cm^2) and an 18.4-fold increase in fixed cells (89.93±6.59 µg/cm^2) after 7 days compared with cells incubated in non-procalcifying medium (1 mmol/L phosphate). However,

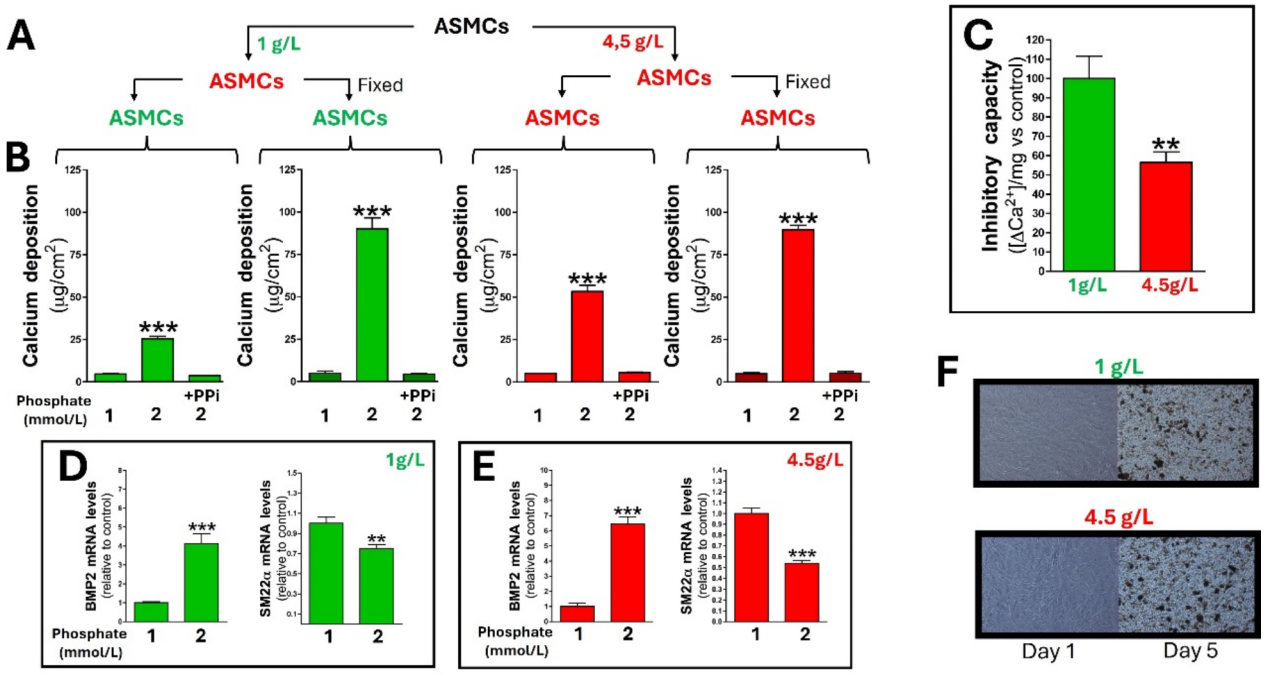

Fig. 5 High glucose levels accelerated phosphate-induced aortic smooth muscle cell calcification. **A** Schematic representation of the experimental setup. Rat ASMCs were incubated in MEM containing either 1 g/L or 4.5 g/L glucose for one month. Following this period, the cells were incubated overnight in MEM containing 0.1% FBS. Some cells were then fixed as detailed in the Methods section. The cells were subsequently incubated in MEM (containing 0.1% FBS) with either 1 mmol/L or 2 mmol/L phosphate in the absence or presence of 100 µmol/L pyrophosphate (+ PPi). After 7 days of incubation, with daily media replacement, the calcium content was measured as described in the Materials and Methods section. **A** Schematic overview of the experimental design for calcification assays. **B** Quantitative measurements of calcium deposition across the four experimental groups. **C** Calcification inhibitory capacity was calculated as the difference in calcium deposition between living and fixed cells (ΔCa^{2+}). **D** and **E** Quantitative PCR analysis of the mRNA levels of BMP2 and SM22α in ASMCs subjected to phosphate-induced calcification and incubated with 1 g/L glucose (**D**) or 4.5 g/L glucose (**E**). **F** Representative microscopy images (10x magnification; scale bar: 100 µm) showing calcification in ASMCs incubated with 1 g/L glucose (top) or 4.5 g/L glucose (bottom). The data are shown as the mean ± SEM from four independent experiments, each with three plates per experiment. Statistical analysis was performed via one-way ANOVA with Tukey's post hoc test (**D, E**) and Student's t test (**B, C**). Asterisks indicate a significant difference with $^{**}P < 0.01$; $^{***}P < 0.001$

ASMCs incubated with a normal glucose concentration (1 g/L) presented a significant 10.7-fold increase in calcium deposition (53.38 ± 3.52 µg/cm²). Despite this, the calcium content in fixed cells under normal glucose conditions was comparable to that observed under high-glucose conditions, showing an 18.6-fold increase. The addition of pyrophosphate to the phosphate-calcifying medium completely prevented calcium accumulation in both fixed and living cells under both glucose conditions.

The ability to inhibit calcification (ΔCa^{2+}, inhibitory capacity) was determined by calculating the difference in calcium deposition between fixed and living cells (Ca^{2+} in fixed cells minus Ca^{2+} in living cells). The ΔCa^{2+} in high-glucose-treated cells was significantly lower (56.38%) than that in control ASMCs (Fig. 5C).

Finally, the expression of two well-known calcification markers was analyzed in cells cultured under phosphate-induced calcification. Figure 5D and E show increased expression of bone morphogenic protein 2 (BMP2) and decreased expression of smooth muscle protein 22-α (SM22α) in calcified cells (2 mmol/L phosphate) compared with noncalcified cells (control, 1 mmol/L phosphate) under both 4.5 g/L glucose (Fig. 5D) and 1 g/L glucose (Fig. 5E) conditions.

STZ-treated rats exhibit impaired pyrophosphate synthesis in the aortic wall

The streptozotocin (STZ) rat model is widely used to induce type 1 diabetes by selectively destroying insulin-producing beta cells in the pancreas, thereby mimicking the pathological characteristics of the disease.

The STZ-induced rat model demonstrated significant weight loss (Fig. 1A), elevated blood glucose levels (Fig. 1B), decreased blood insulin levels (Fig. 1C), and an increase in advanced glycation end products (AGEs, Fig. 1D) one month after a single-dose injection. Moreover, liver glycogen levels (Fig. 1E) are significantly reduced in STZ-treated rats, whereas glycated serum protein (GSP, Fig. 1F) and tumor necrosis factor alpha (TNFα; Fig. 1G) levels are significantly elevated in the blood of these rats. These results support previous

studies and demonstrate the effectiveness of the STZ-induced diabetes model in rats [39–41].

To investigate extracellular pyrophosphate metabolism in the aortic wall, ATP hydrolysis products were also separated via thin layer chromatography. As shown in Fig. 6A, the hydrolysis of 1 µmol/L ATP was complete after 30 min of incubation in rat aortic rings, which is consistent with previous findings [24, 25]. The production of pyrophosphate from ATP hydrolysis was not affected by the addition of a specific TNAP inhibitor (SBI425), suggesting that the liberated pyrophosphate was not hydrolyzed by TNAP during the assay. However, the addition of inorganic phosphatase completely abolished pyrophosphate production (Fig. 6B). Notably, the pyrophosphate-to-phosphate ratio (Fig. 6C) resulting from ATP hydrolysis was significantly lower (2.2-fold) in the aortic rings of the SZT-treated rats (0.13±0.01) than in those of the control rats (0.05±0.0005).

Furthermore, the synthesis of pyrophosphate from ATP hydrolysis was significantly lower in aortic rings from STZ-treated rats (0.83±0.06 pmol*mg^{-1}*min^{-1}) than in those from control rats (1.50±0.06 pmol*mg^{-1}*min^{-1}; Fig. 6D). Additionally, pyrophosphate hydrolysis was markedly greater in aortic rings from SZT-treated rats (0.49±0.05 pmol*mg^{-1}*min^{-1}) than in those from control rats (0.13±0.02 pmol*mg^{-1}*min^{-1}; Fig. 6E).To complement the results obtained for pyrophosphate synthesis and hydrolysis in aortic tissue, we next analyzed the protein levels and mRNA expression of the three main enzymes involved in pyrophosphate metabolism. Figure 6F shows a significant reduction in eNPP1 levels in the aortas of STZ-treated rats. In contrast, both TNAP and eNTPD1 protein levels were significantly elevated in aortas from treated rats compared with those from control rats.

Moreover, analysis of the mRNA expression of the three key enzymes involved in extracellular pyrophosphate metabolism revealed significant upregulation of eNTPD1 (ATP→phosphate) and TNAP (pyrophosphate→phosphate) in STZ-treated rat aortas compared with control aortas (Fig. 6G). Specifically, the mRNA levels of eNTPD1 and TNAP were increased by 5.8-fold and 6.8-fold, respectively. In contrast, eNPP1 (ATP→pyrophosphate) mRNA expression

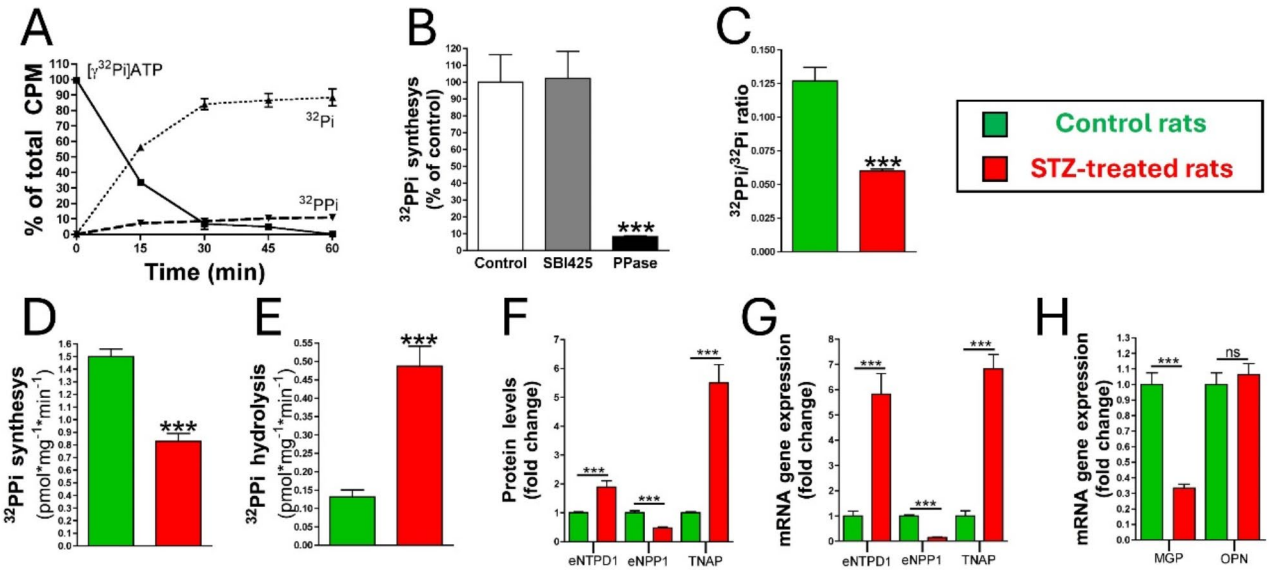

Fig. 6 STZ-treated rats exhibit impaired extracellular pyrophosphate metabolism in the aortic wall. **A** A representative time course of ATP hydrolysis was conducted using a 1 µmol/L ATP solution containing 10 µCi/mL [γ-^{32}P]ATP as a radiotracer. The products of hydrolysis, ^{32}PPi (32-pyrophosphate), ^{32}Pi (32-phosphate), and [γ-^{32}P]ATP-, were separated and quantified via thin layer chromatography, as outlined in the Methods section. **B** The synthesis of pyrophosphate (PPi) was analyzed by hydrolyzing 1 µmol/L ATP containing 10 µCi/mL [γ-^{32}P]ATP as a radiotracer. The reactions were carried out in the absence or presence of either a specific TNAP inhibitor (SBI-425) or inorganic pyrophosphatase (PPase). **C** The ratio of ^{32}PPi to ^{32}Pi generated by ATP hydrolysis was calculated to assess the efficiency and specificity of pyrophosphate synthesis. **D** The synthesis of ^{32}PPi was evaluated by hydrolyzing 1 µmol/L ATP containing 10 µCi/mL [γ-^{32}P]ATP. **E** The release of ^{32}Pi was measured following the hydrolysis of 5 µmol/L pyrophosphate, which contained 10 µCi/mL ^{32}PPi as a radiotracer. **F** Quantification of protein levels via ELISA. **G**, **H** Total RNA was isolated from rat aortas to evaluate the expression levels of key enzymes involved in extracellular pyrophosphate metabolism, including eNTPD1 (ectonucleoside triphosphate diphosphohydrolase 1), eNPP1 (ectonucleotide pyrophosphatase/phosphodiesterase 1), and tissue-nonspecific alkaline phosphatase (TNAP) (panel **G**. Additionally, the expression of calcification-related proteins, such as matrix Gla protein (MGP) and osteopontin (OPN), was assessed (panel H). The data are shown as the mean ± SEM and represent data from 12–16 independent aortas. Statistical analyses were performed via Student's t test. Asterisks indicate a significant difference with ***$P < 0.001$

was significantly reduced, with a 7-fold decrease in SZT-treated rat aortas compared with control aortas. Finally, the mRNA expression of two key anti-calcification proteins was analyzed. The results revealed a significant decrease in matrix Gla protein (MGP) mRNA levels in the aortas of the STZ-treated rats compared with those of the control rats (Fig. 6H). In contrast, osteopontin (OPN) mRNA expression was not significantly different between the two experimental groups.

STZ-treated rats have reduced ATP and pyrophosphate levels in the plasma

Both the plasma ATP (Fig. 7A) and pyrophosphate (Fig. 7B) levels were significantly lower in the STZ-treated rats than in the control rats. Additionally, compared with control rats, STZ-treated rats presented a significant decrease in the pyrophosphate/ATP ratio after one month of incubation (Fig. 7C).

Furthermore, pyrophosphate hydrolysis was significantly increased in the blood of the STZ-treated rats, reaching 233.5±7.71% that of the control rats (Fig. 7D). In addition, the synthesis of pyrophosphate from ATP hydrolysis was markedly lower (42.35±0.87%) in the blood of STZ-treated rats than in that of control rats (Fig. 7E).

STZ-treated rats exhibit a propensity for aortic calcification

Von Kossa or Alizarin Red staining of aortic sections from STZ-treated rats did not reveal a significant increase in calcium after one month of treatment (Fig. 8A). Additionally, calcium quantification in the aortic rings revealed no significant differences between the two experimental groups (Fig. 8B). In contrast, compared with control aortic rings, aortic rings incubated ex vivo significantly increased the accumulation of calcium-45 in STZ-treated aortas, both under phosphate-induced calcification and in control medium (Fig. 8C).

Aortic smooth muscle cells from individuals with type I diabetes exhibit impaired extracellular pyrophosphate metabolism in vitro

Compared with those in non-diabetic hASMCs, extracellular ATP levels in diabetic human ASMCs (hASMCs) significantly decreased to 61.06±2.79% (Fig. 9A). Similarly, compared with those in non-diabetic hASMCs, extracellular pyrophosphate levels (Fig. 9B) in diabetic hASMCs were also significantly lower (41.50±8.05%).

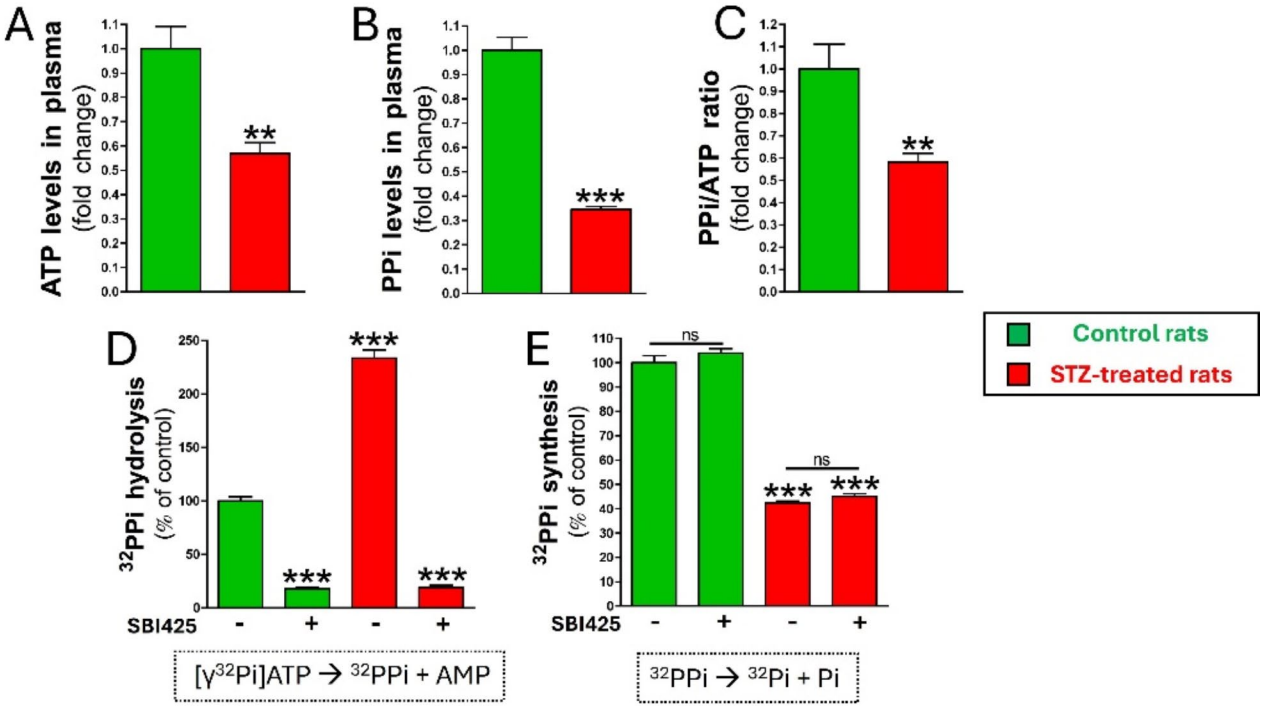

Fig. 7 STZ-treated rats presented reduced ATP and pyrophosphate levels in the plasma. **A** ATP concentration and **B** pyrophosphate (PPi) concentration in plasma were measured in both STZ-treated and untreated rats over 1 month. **C** Pyrophosphate-to-ATP ratio. **D** 32-Pyrophosphate (^{32}PPi) synthesis in blood was assessed via the hydrolysis of 1 µmol/L ATP, containing 10 µCi/mL [γ^{32}Pi]ATP as a radiotracer, in the absence or presence of a specific TNAP inhibitor (SBI425). E) Pyrophosphate hydrolysis was analyzed in blood by measuring the release of 32-phosphate (^{32}Pi) following the hydrolysis of 5 µmol/L pyrophosphate, with 10 µCi/mL ^{32}PPi used as a radiotracer. The results are shown as the mean ± SEM (12 rats per group). Statistical analyses were conducted via Student's t test (**A**, **B**, **C**) or one-way ANOVA with Tukey's post hoc test (**D**, **E**). Asterisks indicate a significant difference with $^{**}P < 0.01$; $^{*}P < 0.001$

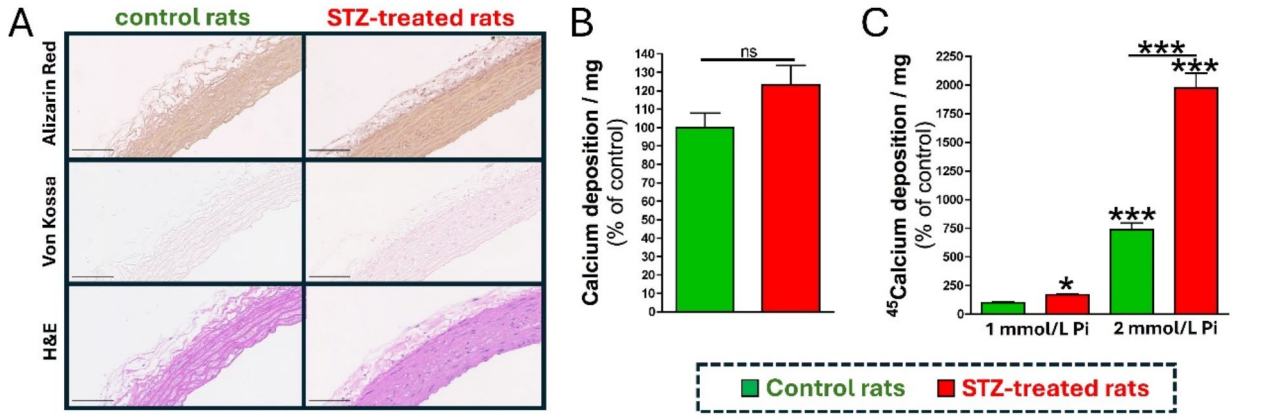

Fig. 8 Increased propensity for calcification in aortas from STZ-treated rats. **A** Representative images (original magnification ×20; scale bar: 100 µm) of H&E, Von Kossa, and Alizarin Red staining images of histological sections of aortic rings from the indicated groups of rats. **B** Calcium content in the aortic rings, expressed as µg of calcium per milligram of dry aorta. "Control" refers to aortas from nontreated rats. **C** Accumulation of calcium-45 (^{45}Calcium) in aortic rings incubated ex vivo for 5 days with 1 mmol/L phosphate and 10 µCi/mL calcium-45 radiotracer. **D** Accumulation of calcium-45 (^{45}Calcium) in aortic rings incubated ex vivo for 5 days with 2 mmol/L phosphate and 10 µCi/mL calcium-45 radiotracer. In both panels (**C** and **D**), "Control" refers to aortas from nontreated rats incubated with 1 mmol/L phosphate. The data are shown as the mean ± SEM (12 aortic rings per group). Statistical analyses were performed via Student's t test, with asterisks indicating significant differences at $^{*}P < 0.001$

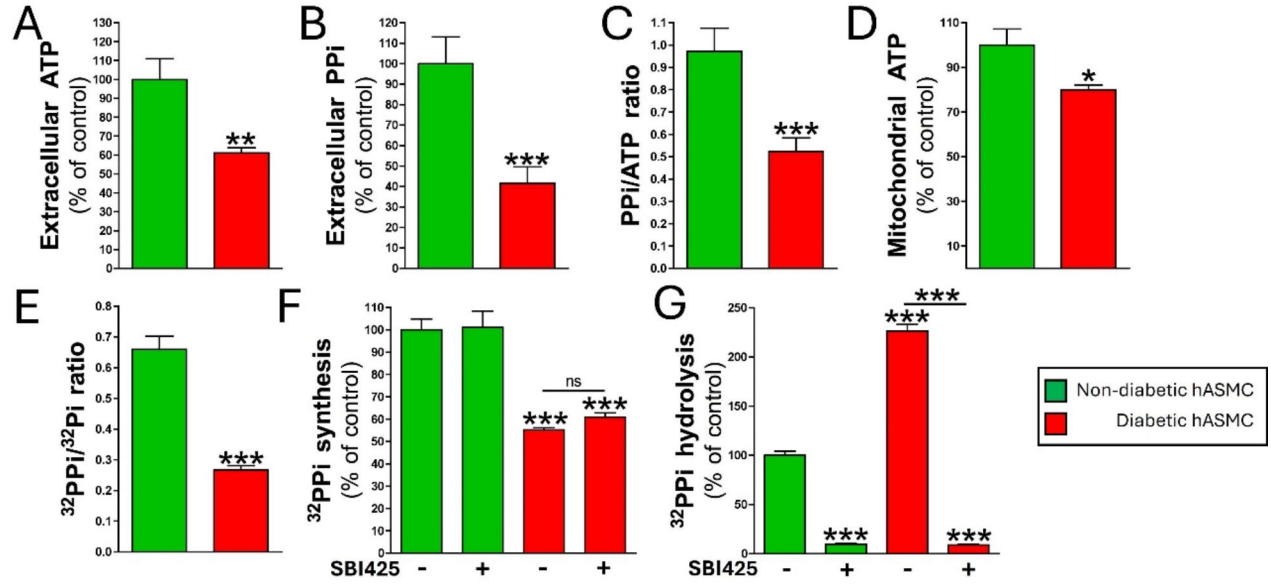

Fig. 9 Diabetic human aortic smooth muscle cells exhibit impaired extracellular pyrophosphate metabolism. **A** Extracellular ATP concentration and **B** extracellular pyrophosphate concentration in human aortic smooth muscle cells from both diabetic and non-diabetic (Control) individuals. **C** Pyrophosphate-to-ATP ratio. **D** Mitochondrial ATP synthesis. **E** 32-Pyrophosphate-to-32-phosphate ratio released by hydrolysis of ATP containing 10 µCi/mL [γ^{32}Pi]ATP as a radiotracer. **F** 32-Pyrophosphate (^{32}PPi) synthesis was evaluated through the hydrolysis of 1 µmol/L ATP, containing 10 µCi/mL [γ^{32}Pi]ATP as a radiotracer, in the absence or presence of a specific TNAP inhibitor (SBI 425). **G** Pyrophosphate hydrolysis was assessed by measuring the release of 32-phosphate (^{32}Pi) following the hydrolysis of 5 µmol/L pyrophosphate, with 10 µCi/mL ^{32}PPi used as a radiotracer. The results are shown as the mean ± SEM ($n = 16$; 4 independent experiments with 4 culture plates per experiment). Statistical analyses were conducted via Student's t test (**A**–**E**) or one-way ANOVA with Tukey's post hoc test (**F**, **G**). Asterisks indicate a significant difference with $^{*}P < 0.05$; $^{**}P < 0.01$; $^{***}P < 0.001$

Notably, the extracellular pyrophosphate/ATP ratio was significantly reduced to 52.27 ± 0.06% in diabetic hASMCs (Fig. 9C), suggesting impaired extracellular pyrophosphate metabolism. Moreover, mitochondrial synthesis of ATP was also significantly lower (79.91 ± 2.25%) in diabetic hASMCs than in non-diabetic hASMCs (Fig. 9D).

To investigate the synthesis and hydrolysis of pyrophosphate in human smooth muscle cells, both diabetic hASMCs and non-diabetic hASMCs were incubated

with [γPi^{32}]ATP to assess pyrophosphate synthesis and with ^{32}PPi to evaluate pyrophosphate hydrolysis. Figure 9E and F show a significant reduction in both the pyrophosphate/phosphate ratio and the synthesis of pyrophosphate via ATP hydrolysis in diabetic hASMCs. In contrast, pyrophosphate hydrolysis was significantly increased 2.2-fold in diabetic hASMCs compared with non-diabetic hASMCs (Fig. 9G).

Aortic smooth muscle cells from individuals with type I diabetes exhibit an increased propensity for calcification

To investigate the impact of the diabetic environment on vascular calcification, both diabetic and non-diabetic hASMCs were incubated in phosphate-calcifying medium (2 mmol/L phosphate) containing calcium-45 (^{45}Ca) as a radiotracer. The calcification induced by phosphate was then evaluated in both live and fixed cells over a 5-day period (Fig. 10). The ability to inhibit calcification (ΔCa^{2+}, inhibitory capacity to prevent calcification) was determined by calculating the difference in calcium deposition between fixed and living cells (Ca^{2+} in fixed cells minus Ca^{2+} in living cells), according to previous methods. In accordance with our previous results, calcium accumulation was significantly greater in diabetic hASMCs than in non-diabetic hASMCs. Finally, the ΔCa^{2+} in diabetic hASMCs was significantly lower (to 75%) than that in non-diabetic hASMCs.

Discussion

Diabetes, particularly type 1 and type 2 diabetes, is closely associated with an increased risk of vascular calcification [7, 10, 42], which is the deposition of calcium phosphate salts in the vascular walls. Vascular calcification is a significant predictor of cardiovascular morbidity and mortality, especially in diabetic patients [43]. This pathological process affects the elasticity and function of blood vessels, contributing to the development of arteriosclerosis, hypertension, and ultimately cardiovascular disease. In the context of diabetes, several mechanisms contribute to the increased propensity for vascular calcification, including hyperglycemia, inflammation, oxidative stress, hormonal imbalance and renal dysfunction.

Pyrophosphate is a critical endogenous inhibitor of vascular calcification [13]. As a key regulatory molecule in mineralization processes, pyrophosphate protects against the spontaneous deposition of calcium phosphate crystals within vascular walls, thereby maintaining vascular compliance and functional integrity. By directly inhibiting the formation of hydroxyapatite, the primary mineral component of calcified tissues, pyrophosphate

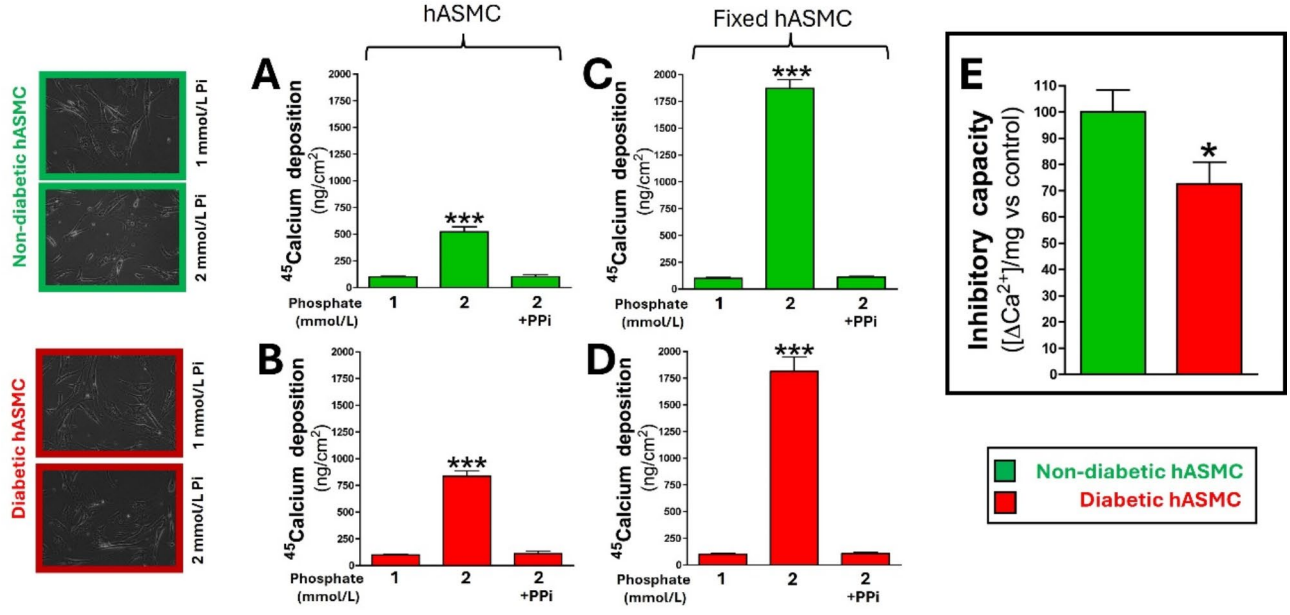

Fig. 10 Reduced inhibitory capacity of diabetic human smooth muscle cells to prevent phosphate-induced calcification. Human non-diabetic and diabetic aortic smooth muscle cells (hASMCs) were grown to confluence as described in the Methods section. Some cells were then fixed as detailed in the same section. The cells were subsequently incubated in MEM containing 10 µCi/mL calcium-45 (^{45}Calcium) as a radiotracer, with either 1 mmol/L or 2 mmol/L phosphate, in the absence or presence of 100 µmol/L pyrophosphate (+PPi). After 4 days of incubation with daily media replacement, the calcium-45 (^{45}Calcium) content was measured as described in the Materials and Methods section. **A** Non-diabetic hASMCs. **B** Fixed non-diabetic hASMCs. **C** Diabetic hASMCs. **D** Fixed diabetic hASMCs. The cells incubated with 1 mmol/L phosphate served as the control. **E** Calcification inhibitory capacity was calculated as the difference in calcium deposition between living and fixed cells (ΔCa^{2+}). The results are shown as the mean ± SEM (four independent experiments, each with three wells per experiment). Statistical analysis was performed via one-way ANOVA with Tukey's post hoc test (**A**-**D**) and Student's t test (**E**). Asterisks indicate significant differences, with *$P < 0.05$ and ***$P < 0.001$

sustains a precise equilibrium between pro-mineralization and anti-mineralization forces within the extracellular matrix. Lower extracellular pyrophosphate levels are associated with accelerated vascular calcification, particularly in metabolic conditions such as chronic kidney disease [21, 44], and accelerated aging [14, 27]. This relationship underscores the potential of pyrophosphate as a crucial factor in mitigating vascular calcification within systemic metabolic disorders, highlighting its importance in vascular health and disease prevention. Although the link between diabetes and vascular calcification is well established, to our knowledge, no studies have specifically investigated the role of extracellular pyrophosphate metabolism in the context of diabetes. Analysis of pyrophosphate levels in diabetic patients could provide valuable insights into the potential role of pyrophosphate in vascular calcification within this population.

Our study highlights a significant disruption in the metabolism of extracellular pyrophosphate in various models of type I diabetes, including glucose-induced diabetic rat ASMCs, STZ-induced diabetic rats, and diabetic human ASMCs. This disruption manifests as a marked reduction in pyrophosphate levels, which compromises the ability of the vascular system to prevent calcification.

In rat ASMCs, the normal synthesis of pyrophosphate is altered under high-glucose conditions, leading to insufficient levels of this critical inhibitor. Similarly, in STZ-induced diabetic rats, we observed a significant decrease in pyrophosphate synthesis coupled with an increase in pyrophosphate hydrolysis. This imbalance results in an environment that favors vascular calcification, further exacerbating the cardiovascular risks associated with diabetes. Moreover, diabetic human ASMCs also exhibit impaired pyrophosphate metabolism. The decreased synthesis and increased breakdown of pyrophosphate in these cells underscore the pervasive impact of diabetes on vascular health. This impairment likely contributes to the heightened propensity for vascular calcification observed in diabetic patients, linking metabolic disturbances directly to the progression of cardiovascular disease.

These results suggest that therapeutic strategies aimed at restoring pyrophosphate levels [14, 45–48] or inhibiting its hydrolysis [49, 50] may potentially mitigate the increased cardiovascular risk associated with vascular calcification in diabetic patients. For example, the administration of exogenous pyrophosphate, either through intraperitoneal injections [14, 45, 46] or high-dose oral supplementation [47, 51], has been shown to reduce ectopic calcification in various experimental models. Furthermore, the pharmacological inhibition of tissue-nonspecific alkaline phosphatase (TNAP) has demonstrated efficacy in preventing calcification in multiple model systems [27, 50]. In addition, targeting eNTPD1 inhibition has also proven effective in reducing calcification, especially within a progeria model [27]. Further investigation into these therapeutic strategies is warranted to rigorously evaluate their efficacy in attenuating vascular calcification and preventing cardiovascular complications in individuals with diabetes.

Previous studies have identified two distinct stages in the process of aortic calcification, particularly in the context of phosphate-induced calcification [25]: an early stage (pre-calcification phase) and a late stage (calcification phase). In the early stage, there is no significant calcium accumulation in cells or tissues. In contrast, the late stage is characterized by visible and measurable calcification. During the late stage, the presence of hydroxyapatite exerts a direct effect on aortic smooth muscle cell biology, leading to alterations in extracellular pyrophosphate metabolism and promoting osteochondrogenic differentiation, as evidenced by increased BMP2 expression and reduced SM22α levels [25, 52]. To assess the impact of high glucose on extracellular pyrophosphate metabolism, the focus has been on studying this process in the early stages to avoid confounding effects from hydroxyapatite accumulation.

In our study, we observed a decrease in the proliferation and viability of ASMCs under high-glucose conditions. Elevated glucose levels can significantly impact cellular proliferation through several interconnected mechanisms. High-glucose conditions increase oxidative stress and promote the formation of AGEs, which impair various cellular functions and reduce cell viability [53]. For example, AGEs have been shown to induce oxidative damage and disrupt normal cellular processes, contributing to decreased proliferation [54]. Moreover, diabetes increases the production of reactive oxygen species, which can damage endothelial cells and promote calcification [55, 56]. Oxidative stress disrupts the balance between pro-calcifying and anti-calcifying factors in the vascular wall, favoring calcification [57].

Prolonged exposure to high glucose can interfere with key signaling pathways that regulate cell cycle progression, effectively slowing or inhibiting cell proliferation. Research indicates that high-glucose conditions can lead to cellular stress responses that negatively affect cell cycle regulators, thereby reducing proliferation rates [58]. High glucose levels can also impair mitochondrial function, leading to a reduction in ATP synthesis [59]. This decrease in the cellular energy supply is critical for proliferation and other vital processes. Consistent with these findings, we also report a reduction in mitochondrial ATP synthesis in rat ASMCs after long-term exposure to high glucose levels, as well as in cells derived from diabetic patients. Importantly, our study revealed an increase in P2Y6 expression. Nucleotides released during inflammatory responses or upon mechanical stimulation

act through the P2 family of nucleotide receptors. In this context, the upregulation of P2Y6 could facilitate ATP release, activating downstream signaling pathways that support cellular survival and function [60, 61]. These findings suggest that P2Y6 may act as a regulator in conditions of cellular stress or inflammation, potentially compensating for impaired mitochondrial ATP synthesis by promoting extracellular ATP release, thereby contributing to increased cellular resilience.

Moreover, high glucose levels can also significantly impact aortic smooth muscle cells by influencing apoptosis, osteogenic differentiation, and the expression of calcification inhibitors. Research indicates that high glucose levels actually inhibit apoptosis in vascular smooth muscle cells. For example, a study demonstrated that high-glucose conditions suppress serum withdrawal–induced apoptosis in ASMCs by increasing the expression of anti-apoptotic proteins such as Bcl-2 and Bcl-xL, suggesting that increased expression of these proteins may play a significant role in the development of macrovascular complications in individuals with diabetes [62]. Additionally, another study revealed that high glucose inhibits ASMC apoptosis through a protein kinase C–dependent pathway, further supporting the notion that elevated glucose levels reduce apoptosis in ASMCs [63]. These findings suggest that high-glucose environments may contribute to vascular dysfunction not by accelerating apoptosis but rather by inhibiting it, potentially leading to abnormal VSMC accumulation and associated vascular complications.

Elevated glucose levels have been linked to increased osteogenic differentiation of vascular smooth muscle cells. Studies indicate that high-glucose conditions upregulate osteogenic markers such as BMP-2 and alkaline phosphatase in vascular smooth muscle cells, suggesting transdifferentiation toward osteoblast-like cells [64]. Our results further support these findings, showing a marked increase in TNAP and BMP-2 expression under high-glucose conditions, reinforcing the role of hyperglycemia in promoting osteogenic transformation and contributing to vascular calcification.

Elevated glucose levels can disrupt the expression of other calcification inhibitors, such as MGP, in vascular smooth muscle cells. The MGP plays a crucial role in preventing abnormal mineral deposition within vascular walls. Studies have shown that high-glucose environments decrease MGP expression in ASMCs, leading to increased calcification and vascular dysfunction [65]. Additionally, research has indicated that hyperglycemia can downregulate MGP expression, further promoting vascular calcification [66]. Our findings align with these observations, as we also identified a significant reduction in MGP expression under high-glucose conditions. Therefore, under hyperglycemic conditions, reduced levels or activity of MGP, either independently or in conjunction with impaired pyrophosphate synthesis, can exacerbate the calcification process, contributing to vascular disease.

Traditionally, pyrophosphate has been recognized as a potent inhibitor of extracellular calcification; however, recent evidence highlights an additional significant role of pyrophosphate as a signaling molecule that modulates gene expression and cellular behavior in mineralizing cells. For example, studies in osteoblasts have shown that pyrophosphate promotes differentiation and upregulates key extracellular matrix genes, including collagen type 1 (COL1), osteopontin, and alkaline phosphatase, particularly at relatively high concentrations [16]. This upregulation suggests that pyrophosphate actively enhances osteogenic potential by stimulating matrix production and maturation. Additional evidence of the signaling role of pyrophosphate has revealed its effects on osteoclasts and osteoblasts, where it not only inhibits bone mineralization but also directly regulates cellular function [18]. For example, prolonged pyrophosphate exposure decreases osteoclast formation and resorptive activity, whereas in osteoblasts, it promotes matrix deposition and collagen synthesis. Moreover, pyrophosphate influences the expression of MGP by regulating pathways involved in extracellular matrix mineralization [19]. This dual function of pyrophosphate—as both a direct inhibitor of crystal growth and a modulator of gene expression related to calcification—offers a new perspective on how pyrophosphate homeostasis may be crucial for preventing pathological calcification and maintaining tissue health.

The authors recognize several limitations in this study, which should be carefully considered when interpreting the results. First, there remains a significant gap in the literature regarding direct evidence of pyrophosphate deficiency in diabetic patients. Although pyrophosphate is well established as a natural inhibitor of vascular calcification, there is no concrete research linking its deficiency explicitly to diabetes. This absence of data restricts the ability to assert a definitive connection between diabetes-induced metabolic dysregulation and reduced pyrophosphate levels, thus limiting the extrapolation of the study's findings to clinical settings.

Second, creating animal models that replicate the gradual vascular calcification observed in diabetic humans over the years is challenging. Short-term models often induce calcification rapidly through aggressive methods that trigger inflammation, stress, and metabolic overload, which diverge from the slower, chronic calcification process in diabetes. Achieving a long-term model that mirrors this progression without excessive external influence is essential for understanding diabetes-specific impacts on vascular health. However, the biological and technical

difficulties in maintaining such models over extended periods limit the ability to fully capture the complex, gradual calcification observed in diabetic patients.

Finally, the heterogeneity of human vascular smooth muscle cell samples introduces an additional level of variability. This variability arises not only from inherent genetic and phenotypic diversity among donors but also from differences in lifestyle, medication use, and other environmental factors. Such diversity can influence cellular responses to high glucose levels, impacting pyrophosphate metabolism and susceptibility to calcification. While this variability mirrors real-world conditions, it may also limit the study's generalizability and reproducibility across a broader diabetic population.

Conclusions

1. Impaired Pyrophosphate Metabolism: Our study demonstrated that pyrophosphate metabolism is significantly impaired in diabetic conditions, including in rat ASMCs, STZ-induced diabetic rats, and diabetic human ASMCs.
2. Increased Propensity for Vascular Calcification: A reduction in extracellular pyrophosphate levels creates an environment conducive to vascular calcification. This is particularly evident in diabetic models where pyrophosphate metabolism is disrupted, highlighting the direct link between diabetes and an increased risk of vascular calcification.
3. Potential therapeutic targets: The findings suggest that interventions aimed at restoring or enhancing pyrophosphate levels could serve as novel therapeutic strategies to combat vascular calcification in diabetic patients.

Author contributions.

AFR, BML, and RVB conducted the experiments. RVB provided the materials and drafted the manuscript. All the authors reviewed and approved the final version of the manuscript.

Funding.

This study was supported by grants from the Spanish Ministry of Education and Science (SAF-2014-60699-JIN and PID2020-113603RD-100), the Spanish Society of Nephrology (SEN21-3315), and the Xunta de Galicia (ED431F 2022/03). Additional support was provided through a Senior Research contract under the Ramón y Cajal program from the Spanish Government (RYC2019-027920-I to RVB), a predoctoral fellowship from the Spanish Government (FPI PRE2021-100795 to AFR), and a predoctoral fellowship from the Xunta de Galicia (ED481A 2022/383 to BML).

Declarations.

Competing interests The authors declare that they have no competing interests.

Ethical approval and consent to participate Not applicable.

Consent for publication Not applicable.

Abbreviations

AGEs	Advanced glycation end products
AMP	Adenosine-5′-monophosphate
ANK	Progressive ankylosis gene
ASMCs	Primary aortic smooth muscle cells
ATP	Adenosine-5′-triphosphate
BMP2	Bone morphogenic protein 2
BrdU	5-Bromodeoxyuridine
CPCs	Calcium phosphate crystals
eNPP1	Ectonucleotide pyrophosphatase/phosphodiesterase 1
eNTPD1	Ectonucleoside triphosphate diphosphohydrolase 1
GSP	Glycated serum protein
MGP	Matrix gla protein
OPN	Osteopontin
Pi	Inorganic phosphate
Pit1	Type III transporter sodium phosphate cotransporter 1 (SLC20A1)
Pit2	Type III transporter sodium phosphate cotransporter 2 (SLC20A2)
PPi	Inorganic pyrophosphate
P2Y2	P2Y purinoceptor 2
P2Y6	P2Y purinoceptor 6
RAGE	Receptor for advanced glycation end products
ROS	Reactive oxygen species
RUNX2	Runt-related transcription factor 2
SBI425	Specific TNAP inhibitor
STZ	Streptozotocin
SM22α	Smooth muscle protein 22-α
TLC	Thin-layer chromatography
TNAP	Tissue-nonspecific alkaline phosphatase
TNFα	Tumor necrosis factor alpha
5NT	5′-Nucleotidase

Acknowledgements

The authors express their gratitude for the assistance provided by the staff of the animal facility.

Author contributions

AFR, BML, and RVB conducted the experiments. RVB provided the materials and drafted the manuscript. All authors have reviewed and approved the final version of the manuscript.

Data availability

No datasets were generated or analysed during the current study.

Declarations

Competing interests

The authors declare no competing interests.

Author details

[1]Center for Research in Molecular Medicine and Chronic Diseases (CiMUS). Campus Vida, University of Santiago de Compostela, 15782 Santiago de Compostela, Spain
[2]Health Research Institute of Santiago de Compostela (IDIS), Travesia da Choupana S/N, 15706 Santiago de Compostela, Spain
[3]Department of Biochemistry and Molecular Biology, University of Santiago de Compostela, 15782 Santiago de Compostela, Spain
[4]Center for Research in Molecular Medicine and Chronic Diseases (CiMUS). Campus Vida, University of Santiago de Compostela, Avenida de Barcelona S/N, 15782 Santiago de Compostela, Spain

Received: 11 September 2024 / Accepted: 4 November 2024

Published online: 11 November 2024

References

1. Cloete L. Diabetes mellitus: an overview of the types, symptoms, complications and management. Nurs Stand R Coll Nurs G B 1987. 2022;37(1):61–6.
2. Bielka W, Przezak A, Molęda P, Pius-Sadowska E, Machaliński B. Double diabetes-when type 1 diabetes meets type 2 diabetes: definition, pathogenesis and recognition. Cardiovasc Diabetol. 2024;23(1):62.
3. Cole JB, Florez JC. Genetics of diabetes mellitus and diabetes complications. Nat Rev Nephrol j. 2020;16(7):377–90.
4. Strain WD, Paldánius PM. Diabetes, cardiovascular disease and the microcirculation. Cardiovasc Diabetol. 2018;17(1):57.
5. Wong ND, Sattar N. Cardiovascular risk in diabetes mellitus: epidemiology, assessment and prevention. Nat Rev Cardiol. 2023;20(10):685–95.
6. Rutsch F, Nitschke Y, Terkeltaub R. Genetics in arterial calcification: pieces of a puzzle and cogs in a wheel. Circ Res. 2011;109(5):578–92.
7. Dal Canto E, Ceriello A, Rydén L, Ferrini M, Hansen TB, Schnell O, et al. Diabetes as a cardiovascular risk factor: an overview of global trends of macro and micro vascular complications. Eur J Prev Cardiol. 2019;26(2suppl):25–32.
8. An Y, Xu BT, Wan SR, Ma XM, Long Y, Xu Y, et al. The role of oxidative stress in diabetes mellitus-induced vascular endothelial dysfunction. Cardiovasc Diabetol. 2023;22(1):237.
9. Yao H, Sun Z, Zang G, Zhang L, Hou L, Shao C, et al. Epidemiological Research Advances in vascular calcification in diabetes. J Diabetes Res. 2021;2021:4461311.
10. Yahagi K, Kolodgie FD, Lutter C, Mori H, Romero ME, Finn AV, et al. Pathology of Human Coronary and Carotid Artery atherosclerosis and vascular calcification in diabetes Mellitus. Arterioscler Thromb Vasc Biol. 2017;37(2):191–204.
11. Villa-Bellosta R. Role of the extracellular ATP/pyrophosphate metabolism cycle in vascular calcification. Purinergic Signal. 2023;19(2):345–52.
12. Villa-Bellosta R. New insights into endogenous mechanisms of protection against arterial calcification. Atherosclerosis. 2020;306:68–74.
13. Villa-Bellosta R, O'Neill WC. Pyrophosphate deficiency in vascular calcification. Kidney Int. 2018;93(6):1293–7.
14. Villa-Bellosta R, Rivera-Torres J, Osorio FG, Acín-Pérez R, Enriquez JA, López-Otín C, et al. Defective extracellular pyrophosphate metabolism promotes vascular calcification in a mouse model of Hutchinson-Gilford progeria syndrome that is ameliorated on pyrophosphate treatment. Circulation. 2013;127(24):2442–51.
15. Villa-Bellosta R, Egido J. Phosphate, pyrophosphate, and vascular calcification: a question of balance. Eur Heart J. 2017;38(23):1801–4.
16. Pujari-Palmer M, Pujari-Palmer S, Lu X, Lind T, Melhus H, Engstrand T, et al. Pyrophosphate stimulates differentiation, Matrix Gene expression and alkaline phosphatase activity in Osteoblasts. PLoS ONE. 2016;11(10):e0163530.
17. Svensson S, Palmer M, Svensson J, Johansson A, Engqvist H, Omar O, et al. Monocytes and pyrophosphate promote mesenchymal stem cell viability and early osteogenic differentiation. J Mater Sci Mater Med. 2022;33(1):11.
18. Bourne LE, Davies BK, Millan JL, Arnett TR, Wheeler-Jones CPD, Keen JAC, et al. Evidence that pyrophosphate acts as an extracellular signaling molecule to exert direct functional effects in primary cultures of osteoblasts and osteoclasts. Bone. 2023;176:116868.
19. Addison WN, Azari F, Sørensen ES, Kaartinen MT, McKee MD. Pyrophosphate inhibits mineralization of osteoblast cultures by binding to mineral, upregulating osteopontin, and inhibiting alkaline phosphatase activity. J Biol Chem. 2007;282(21):15872–83.
20. Lomashvili KA, Garg P, Narisawa S, Millan JL, O'Neill WC. Upregulation of alkaline phosphatase and pyrophosphate hydrolysis: potential mechanism for uremic vascular calcification. Kidney Int. 2008;73(9):1024–30.
21. Azpiazu D, González-Parra E, Egido J, Villa-Bellosta R. Hydrolysis of Extracellular Pyrophosphate increases in post-hemodialysis plasma. Sci Rep. 2018;8(1):11089.
22. Zimmermann H. Extracellular metabolism of ATP and other nucleotides. Naunyn Schmiedebergs Arch Pharmacol. 2000;362(4–5):299–309.
23. Zimmermann H, Zebisch M, Sträter N. Cellular function and molecular structure of ecto-nucleotidases. Purinergic Signal. 2012;8(3):437–502.
24. Villa-Bellosta R, Wang X, Millán JL, Dubyak GR, O'Neill WC. Extracellular pyrophosphate metabolism and calcification in vascular smooth muscle. Am J Physiol Heart Circ Physiol. 2011;301(1):H61–68.
25. Villa-Bellosta R. Synthesis of Extracellular Pyrophosphate increases in vascular smooth muscle cells during phosphate-Induced calcification. Arterioscler Thromb Vasc Biol. 2018;38(9):2137–47.
26. Rutsch F, Ruf N, Vaingankar S, Toliat MR, Suk A, Höhne W, et al. Mutations in ENPP1 are associated with «idiopathic» infantile arterial calcification. Nat Genet. 2003;34(4):379–81.
27. Villa-Bellosta R. ATP-based therapy prevents vascular calcification and extends longevity in a mouse model of Hutchinson-Gilford progeria syndrome. Proc Natl Acad Sci USA. 2019;116(47):23698–704.
28. Villa-Bellosta R, Sorribas V. Prevention of vascular calcification by polyphosphates and nucleotides- role of ATP. Circ J. 2013;77(8):2145–51.
29. Ho AM, Johnson MD, Kingsley DM. Role of the mouse ank gene in control of tissue calcification and arthritis. Science. 2000;1(5477):265–70.
30. Chen NX, Moe SM. Pathophysiology of vascular calcification. Curr Osteoporos Rep. 2015;13(6):372–80.
31. Shanahan CM, Crouthamel MH, Kapustin A, Giachelli CM. Arterial calcification in chronic kidney disease: key roles for calcium and phosphate. Circ Res. 2011;109(6):697–711.
32. Villa-Bellosta R, Hamczyk MR. Isolation and culture of Aortic Smooth Muscle Cells and in Vitro Calcification Assay. Methods Mol Biol Clifton NJ. 2015;1339:119–29.
33. Baqi Y, Weyler S, Iqbal J, Zimmermann H, Müller CE. Structure-activity relationships of anthraquinone derivatives derived from bromaminic acid as inhibitors of ectonucleoside triphosphate diphosphohydrolases (E-NTPDases). Purinergic Signal. 2009;5(1):91–106.
34. Ibanez G, Shum D, Blum G, Bhinder B, Radu C, Antczak C, et al. A high throughput scintillation proximity imaging assay for protein methyltransferases. Comb Chem High Throughput Screen. 2012;15(5):359–71.
35. Pinkerton AB, Sergienko E, Bravo Y, Dahl R, Ma CT, Sun Q, et al. Discovery of 5-((5-chloro-2-methoxyphenyl)sulfonamido)nicotinamide (SBI-425), a potent and orally bioavailable tissue-nonspecific alkaline phosphatase (TNAP) inhibitor. Bioorg Med Chem Lett. 2018;28(1):31–4.
36. Sheen CR, Kuss P, Narisawa S, Yadav MC, Nigro J, Wang W, et al. Pathophysiological role of vascular smooth muscle alkaline phosphatase in medial artery calcification. J Bone Min Res. 2015;30(5):824–36.
37. Villa-Bellosta R. Dietary magnesium supplementation improves lifespan in a mouse model of progeria. EMBO Mol Med. 2020;12(10):e12423.
38. Villa-Bellosta R, Millan A, Sorribas V. Role of calcium-phosphate deposition in vascular smooth muscle cell calcification. Am J Physiol Cell Physiol. 2011;300(1):C210–220.
39. Yang B, Luo Y, Wei X, Kan J. Polysaccharide from Hovenia dulcis (Guaizao) improves pancreatic injury and regulates liver glycometabolism to alleviate STZ-induced type 1 diabetes mellitus in rats. Int J Biol Macromol. 2022;214:655–63.
40. Akinlade OM, Owoyele BV, Soladoye AO. Streptozotocin-induced type 1 and 2 diabetes in rodents: a model for studying diabetic cardiac autonomic neuropathy. Afr Health Sci. 2021;21(2):719–27.
41. Zhang Yzhuo, Fan M ling, Zhang W, zhe, Liu W, Li H ping, Ren S et al. Schisandrin ameliorates diabetic nephropathy by regulating PI3K/Akt/NF-κB-mediated inflammation and TGF-β1-induced fibrosis in HFD/STZ-induced C57BL/6J mice. J Funct Foods. 2023;100:105376.
42. Wang X, Wang Z, He J. Similarities and Differences of Vascular Calcification in diabetes and chronic kidney disease. Diabetes Metab Syndr Obes Targets Ther. 2024;17:165–92.
43. Avogaro A, Rattazzi M, Fadini GP. Ectopic calcification in diabetic vascular disease. Expert Opin Ther Targets. 2014;18(5):595–609.
44. Lomashvili KA, Khawandi W, O'Neill WC. Reduced plasma pyrophosphate levels in hemodialysis patients. J Am Soc Nephrol JASN. 2005;16(8):2495–500.
45. Riser BL, Barreto FC, Rezg R, Valaitis PW, Cook CS, White JA, et al. Daily peritoneal administration of sodium pyrophosphate in a dialysis solution prevents the development of vascular calcification in a mouse model of uremica. Nephrol Dial Transpl. 2011;26(10):3349–57.
46. O'Neill WC, Lomashvili KA, Malluche HH, Faugere MC, Riser BL. Treatment with pyrophosphate inhibits uremic vascular calcification. Kidney Int. 2011;79(5):512–7.
47. Dedinszki D, Szeri F, Kozák E, Pomozi V, Tőkési N, Mezei TR, et al. Oral administration of pyrophosphate inhibits connective tissue calcification. EMBO Mol Med. 2017;9(11):1463–70.
48. Pomozi V, Brampton C, van de Wetering K, Zoll J, Calio B, Pham K, et al. Pyrophosphate supplementation prevents chronic and acute calcification in ABCC6-Deficient mice. Am J Pathol. 2017;187(6):1258–72.

49. Li Q, Huang J, Pinkerton AB, Millan JL, van Zelst BD, Levine MA, et al. Inhibition of tissue-nonspecific alkaline phosphatase attenuates ectopic mineralization in the Abcc6-/- mouse model of PXE but not in the Enpp1 mutant mouse models of GACI. J Invest Dermatol. 2019;139(2):360–8.
50. Narisawa S, Harmey D, Yadav MC, O'Neill WC, Hoylaerts MF, Millán JL. Novel inhibitors of alkaline phosphatase suppress vascular smooth muscle cell calcification. J Bone Min Res off J Am Soc Bone Min Res. 2007;22(11):1700–10.
51. Kozák E, Fülöp K, Tőkési N, Rao N, Li Q, Terry SF et al. Oral supplementation of inorganic pyrophosphate in pseudoxanthoma elasticum. Exp Dermatol. 2021;31(4):548-55.
52. Steitz SA, Speer MY, Curinga G, Yang HY, Haynes P, Aebersold R, et al. Smooth muscle cell phenotypic transition associated with calcification: upregulation of Cbfa1 and downregulation of smooth muscle lineage markers. Circ Res. 2001;89(12):1147–54.
53. Khalid M, Petroianu G, Adem A. Advanced Glycation End products and Diabetes Mellitus: mechanisms and perspectives. Biomolecules. 2022;12(4):542.
54. Chen Y, Meng Z, Li Y, Liu S, Hu P, Luo E. Advanced glycation end products and reactive oxygen species: uncovering the potential role of ferroptosis in diabetic complications. Mol Med Camb Mass. 2024;30(1):141.
55. Domingueti CP, Dusse LMS, Carvalho M das, de Sousa G, Gomes LP, Fernandes KB. Diabetes mellitus: the linkage between oxidative stress, inflammation, hypercoagulability and vascular complications. J Diabetes Complications. 2016;30(4):738–45.
56. Darenskaya MA, Kolesnikova LI, Kolesnikov SI. Oxidative stress: pathogenetic role in diabetes Mellitus and its complications and therapeutic approaches to correction. Bull Exp Biol Med. 2021;171(2):179–89.
57. Tóth A, Balogh E, Jeney V. Regulation of vascular calcification by reactive oxygen species. Antioxid Basel Switz. 2020;9(10):963.
58. Chiu CC, Cheng KC, Lin YH, He CX, Bow YD, Li CY, et al. Prolonged exposure to high glucose induces premature senescence through oxidative stress and autophagy in retinal pigment epithelial cells. Arch Immunol Ther Exp (Warsz) De. 2023;71(1):21.
59. Blagov A, Nedosugova L, Kirichenko T, Sukhorukov V, Melnichenko A, Orekhov A. Mitochondrial dysfunction as a Factor of Energy Metabolism Disorders in type 2 diabetes Mellitus. Front Biosci Sch Ed. 2024;16(1):5.
60. Korcok J, Raimundo LN, Du X, Sims SM, Dixon SJ. P2Y6 nucleotide receptors activate NF-kappaB and increase survival of osteoclasts. J Biol Chem. 2005;280(17):16909–15.
61. Carneiro I, Timóteo MA, Silva I, Vieira C, Baldaia C, Ferreirinha F, et al. Activation of P2Y6 receptors increases the voiding frequency in anesthetized rats by releasing ATP from the bladder urothelium. Br J Pharmacol. 2014;171(14):3404–19.
62. Li H, Télémaque S, Miller RE, Marsh JD. High glucose inhibits apoptosis induced by serum deprivation in vascular smooth muscle cells via upregulation of Bcl-2 and bcl-xl. Diabetes. 2005;54(2):540–5.
63. Hall JL, Matter CM, Wang X, Gibbons GH. Hyperglycemia inhibits vascular smooth muscle cell apoptosis through a protein kinase C-dependent pathway. Circ Res. 2000;87(7):574–80.
64. Zhang F, Guo X, Xia Y, Mao L. An update on the phenotypic switching of vascular smooth muscle cells in the pathogenesis of atherosclerosis. Cell Mol Life Sci CMLS. 2021;79(1):6.
65. Chen NX, Duan D, O'Neill KD, Moe SM. High glucose increases the expression of Cbfa1 and BMP-2 and enhances the calcification of vascular smooth muscle cells. Nephrol Dial Transpl. 2006;21(12):3435–42.
66. Kiselova-Kaneva YD, Nazifova-Tasinova N, Vankova D, Nikolova M, Pasheva M, Yotov Y, et al. Matrix Gla-protein expression in peripheral blood mononuclear cells is related to risk factors in cardiovascular diseased patients. Turk J Biochem. 2022;47(3):247–55.

Publisher's note